

## Durham Research Online

---

### Deposited in DRO:

21 January 2015

### Version of attached file:

Accepted Version

### Peer-review status of attached file:

Peer-reviewed

### Citation for published item:

Brown, R.J. and Blake, S. and Thordarson, T. and Self, S. (2014) 'Pyroclastic edifices record vigorous lava fountains during the emplacement of a flood basalt flow field, Roza Member, Columbia River Basalt Province, USA.', *Geological Society of America bulletin.*, 126 (7-8). pp. 875-891.

### Further information on publisher's website:

<https://doi.org/10.1130/B30857.1>

### Publisher's copyright statement:

---

### Use policy

The full-text may be used and/or reproduced, and given to third parties in any format or medium, without prior permission or charge, for personal research or study, educational, or not-for-profit purposes provided that:

- a full bibliographic reference is made to the original source
- a [link](#) is made to the metadata record in DRO
- the full-text is not changed in any way

The full-text must not be sold in any format or medium without the formal permission of the copyright holders.

Please consult the [full DRO policy](#) for further details.

**Pyroclastic deposits and volcanic edifices record unusually vigorous lava  
fountains during the emplacement of a flood basalt flow field (The Roza Member,  
Columbia River Basalt Province, USA)**

Richard J. Brown<sup>\*</sup>, S. Blake, T. Thordarson<sup>1</sup>, S. Self

Volcano Dynamics Group, Department of Environment, Earth and Ecosystems, The Open  
University, Walton Hall, Milton Keynes, MK7 6AA, UK

<sup>1</sup>School of Geosciences, Grant Institute, The King's Buildings, University of Edinburgh, West Mains  
Road, Edinburgh, EH9 3JW, UK

<sup>\*</sup>Now at: Department of Earth Sciences, Durham University, Science Labs, Durham, DH1 3LE, UK

Contact email: richard.brown3@durham.ac.uk

**Abstract**

The 1300 km<sup>3</sup> tholeiitic lava flow field of the 14.7 Ma Roza Member of the Miocene Columbia River Basalt Group has the best preserved vent system of any known continental flood basalt. Detailed geological mapping and sedimentary logging of the pyroclastic rocks along the >180 km-long vent system has enabled the reconstruction of exposed pyroclastic edifices (partial cones) that built-up around vents. The pyroclastic edifices differ from those constructed during typical basaltic effusive eruptions and may represent a new type of volcanic cone ('agglutinate cones'). They are characterised by low to moderate slope angles (<19°), are composed dominantly of coarse-grained moderately to densely agglutinated and welded spatter and scoria extending up to 750 m away from the vent and had minimum heights of 15–160 m. Thick, well-sorted fall deposits composed of moderately to highly vesicular scoria lapilli extend away from some vents and exhibit some characteristics comparable to the proximal deposits of violent Strombolian or basaltic Plinian

26 eruptions. The recorded volcanic activity does not fit with presently known eruption styles of basaltic  
27 magmas and the evidence indicates that the Roza eruption was punctuated by eruptive activity of  
28 unusually high intensity that was characterised by vigorous lava fountains. The extensive  
29 agglutinated deposits accumulated around the vents as a result of fallout from high ( $>>1$  km)  
30 fountains enhanced by fallout from the lower parts of tall convective columns that rose above the  
31 fountains.

32

33 **Keywords:** flood basalt, pyroclastic, lava fountain, fissure, volcanic vent

34

## 35 **Introduction**

36 Flood basalt eruptions are the most voluminous and longest-lived volcanic events on the planet.  
37 Throughout geological time, periodic flare-ups of flood basalt activity have paved large areas of the  
38 Earth with lava ( $10^6$  km<sup>2</sup>). Due to the huge volume of basalt magma emitted during these eruptions  
39 ( $100\text{s}–1000\text{s km}^3$ ), and the release of massive amounts of climate-altering gases, these events have  
40 been proposed as potential triggers of global climate change and mass extinctions (e.g., Rampino and  
41 Stothers, 1988; Thordarson and Self, 1996; Olsen, 1999; Courtillot and Renne, 2003; Saunders and  
42 Reichow, 2009; Thordarson et al., 2009). These volatiles released from the magma are intruded into  
43 the atmosphere either within ash-bearing eruption plumes or by thermal convection (gas-laden  
44 plumes) above pyroclastic fountains (Stothers et al., 1986; Woods, 1993). The height these climate-  
45 changing gases reach into the atmosphere along with the duration of eruptions are critical for the  
46 longevity and severity of their effect on regional and global climate systems. The deposits of plumes  
47 and fountains from fissure eruptions in continental flood basalt provinces have remained elusive due  
48 to limited exposure and the huge size of most provinces: proximal pyroclastic deposits may account  
49 for  $<0.001$  % of the area covered by a flood basalt flow field and have little chance of being exposed  
50 through erosion (see review in Ross et al., 2005).

51           The best known examples of proximal pyroclastic deposits are from flood basalt fissure  
52   eruptions from the Miocene Columbia River Basalt Province (CRBP), USA. Swanson et al. (1975)  
53   documented vent deposits and related products for two flood basalt flow fields, the Roza Member  
54   and the Ice Harbor Member, and others have since been found (e.g., Reidel and Tolan, 1992). The  
55   products comprise shallow-level dikes (10–>600 m paleo-depths) and a range of pyroclastic deposits  
56   that form pyroclastic cones and sheet-like fall deposits. Elsewhere proximal deposits have proven  
57   useful in deciphering the dynamics of an eruption—something notably lacking for flood basalt  
58   volcanism. In this paper, we present the results of detailed field investigations on the best preserved  
59   proximal deposits of any known flood basalt eruption: the 15 Ma Roza Member (Martin, 1989;  
60   Thordarson and Self, 1996, 1998). We report the results of geological mapping, sedimentary logging  
61   and laboratory investigations of the pyroclastic deposits exposed along the >180 km-long Roza vent  
62   system. We use this data to reconstruct the volcanic edifices that built-up around the vents during the  
63   eruption, and we then discuss what they tell us about near-vent processes during flood basalt  
64   eruptions. We show how the Roza vent system as a whole is comparable to those constructed during  
65   historic basaltic fissure eruptions on Iceland. But we demonstrate that the edifices are markedly  
66   different to those constructed during Hawaiian-Strombolian style monogenetic eruptions (i.e., spatter  
67   or scoria cones) in both morphology and lithology. Indeed, they may constitute a new type of  
68   volcanic landform (here termed ‘agglutinate cones’) characterised by moderate slopes (<20°) and by  
69   being composed of predominantly welded and agglutinated scoria and spatter layers that extend >500  
70   m away from the vent in some cases. We propose that they formed during eruptions that were  
71   typified by periodic vigorous lava fountaining and associated strongly convecting plumes that may  
72   have exceeded Subplinian intensities at some fissure vents. The geological evidence presented  
73   suggests that flood basalt eruptions were periodically capable of transporting climate-changing gas  
74   species high into the atmosphere (Stothers et al., 1986; Thordarson and Self, 1996).

75

## 76 *Geological Setting*

77 The intermontane Miocene CRBP consists of  $> 230\,000\text{ km}^3$  of basalt lava (Camp et al., 2003).  
78 Surface effusion of what are classed as CRB lavas was initiated c. 17 Ma ago in the Steens Mountain  
79 area in Oregon following impingement of the Yellowstone hotspot on the western edge of North  
80 American lithosphere (Camp and Ross, 2004). Lavas were possibly fed by 300 km-long dike swarms  
81 that originated in 15–30 km deep crustal chambers in east-central Oregon/west-central Idaho (Wolff  
82 et al., 2008; Fig. 1A). The last CRBP eruptions occurred in the central part of the CRBP at 6 Ma (the  
83 Pasco Basin; Tolan et al., 1989; Tolan et al., 2009).

84 The crust under the CRBP in SE Washington is composed of complex accreted Late  
85 Paleozoic and Mesozoic intraoceanic terranes and Proterozoic continental crust. Accretion is thought  
86 to have occurred from 135–90 Ma (e.g., Lund and Snee, 1988). The boundary between accreted  
87 terranes and continental crust is a complex suture zone—the Western Idaho Suture Zone (WISZ).  
88 Oblique subduction of the Juan de Fuca plate generated horizontal NNW–SSE compression and E–  
89 W extension during the Miocene, which resulted in NNW–SSE propagation directions for CRBP  
90 magma in dikes through Oregon and SE Washington (Reidel, 1984; Hooper and Conrey, 1989).

91

## 92 **Methods**

93 Pyroclastic deposits were mapped at a 1:5000 scale and geospatial data were recorded on a hand-held  
94 GPS. Detailed measured sections were made of well-exposed outcrops. Conventional methods of  
95 grainsize analysis are not applicable due to agglutination, and the variable degree (low to moderate)  
96 of alteration and lithification seen in most outcrops. One-hundred-and-fifty samples were taken for  
97 rock density measurements, which were carried out in the laboratory following the method outlined  
98 by Houghton and Wilson (1989). At many locations the bedding dips and strikes define partial  
99 pyroclastic edifices. Horizontal dimensions for these edifices are estimated and given as radius

100 (orthogonal to inferred alignment of the vent system) and length (parallel to inferred axis of vent  
101 system).

102 The best exposures are man-made sections, either road or rail cuts or quarries. Most natural  
103 outcrops occur along the floors of glacial flood channels (the ‘channelled scabland’), and lack  
104 exposure of the tops and bottoms of units. Mapping individual fall horizons over more than a few 10s  
105 meters to 100 m is difficult because of intermittent exposure and rapid lateral and vertical gradations,  
106 on a decimeter to a meter scale, from loose scoria through to lava-like densely welded spatter that  
107 lacks outlines of constituent clasts.

108

### 109 **The Roza Member vent system**

110 The 14.7 Ma Roza Member is a 1300 km<sup>3</sup> flood tholeiitic basalt flow field covering ~ 40 300 km<sup>2</sup> of  
111 SE Washington and NE Oregon (Martin, 1989; Tolan et al., 1989; Thordarson and Self, 1998). It  
112 was erupted from a linear vent system (Fig. 1) that presently outcrops discontinuously for >180 km  
113 from just north of Enterprise in NE Oregon to north of Rock Creek in SE Washington (see also  
114 Swanson et al., 1975). It can be divided into two segments: south and north of the Snake River.  
115 South of the Snake River, the vent system is represented by dikes trending N17°W, pyroclastic  
116 deposits and clastogenic lavas. Pyroclastic deposits and proximal lavas are generally poorly exposed  
117 south of the Snake River (Fig. 1A) and consist of thick accumulations of spatter, pyroclastic breccia,  
118 spongy pāhoehoe lobes, and thin to thick, dense lava. In some cases these form small (from ~ 1 to 2  
119 km wide) shield-like edifices (e.g., Little Butte and Big Butte, Swanson et al., 1975).

120 North of the Snake River, the location of the Roza Member vent system is recorded by  
121 proximal pyroclastic deposits and spongy pāhoehoe lavas that accumulated around vents along  
122 fissures (Swanson et al., 1975). They are better exposed than outcrops south of the Snake River  
123 because of the scouring by the great Pleistocene-age Missoula Lake floods (Bretz et al., 1956). In  
124 this study eight new vent areas have been recognised at the NW end of the vent system (Fig. 1B),

125 bringing the total number of exposed fissure-vent segments recorded north of the Snake River to  
126 eleven (including those of Swanson et al., 1975). These pyroclastic accumulations have an apparent  
127 spacing of 1–5 km, although this is somewhat controlled by the degree of exposure, and more are  
128 potentially buried under younger lavas and other deposits (e.g., Pleistocene-Recent glacial loess).  
129 The discovery of new vent deposits to the north of those identified by Swanson et al. (1975) now  
130 clearly indicates that the Roza fissure north of the Snake River strikes N40°W. The pyroclastic  
131 deposits outcrop within a 3 km-wide along-strike zone. Projecting this N40°W trend south-  
132 eastwards, it intersects dikes that trend N20°W–N30°W along the banks of the Snake River,  
133 indicating a 23° counter-clockwise deflection of the dike-vent system over an along-strike distance  
134 of < 5–10 km (Fig. 1B).

135

### 136 **Proximal pyroclastic deposits**

137 A complete spectrum of pyroclastic lithofacies is exposed along the Roza vent system, from loose  
138 scoria fall deposits through to densely welded spatter and clastogenic lava. Lithofacies have been  
139 drawn out of this spectrum of deposits on the basis of composition, texture, rock density, grainsize,  
140 and clast aspect ratio. Lithofacies descriptions and interpretations are summarised in Table 1 and  
141 representative photographs are given in Figure 2. When exposed, pyroclastic deposits are in general  
142 well preserved and are only weakly to moderately altered (mostly clay replacing glass). Primary  
143 textures (e.g., vesicles) and features (e.g., achneliths) are well preserved in some outcrops (Fig. 3B).  
144 The locations of individual Roza vents have been constrained primarily by: (A) a lithofacies  
145 association that comprises scoria, moderately to densely agglutinated scoria and spatter, lava-like  
146 densely welded spatter and clastogenic lava; (B) dipping strata that defines pyroclastic edifices; and  
147 (C) the presence of abundant spatter bombs up to 1 m in diameter indicating deposition under a  
148 fountain. In this paper we follow the terminology outlined by Wolff and Sumner (2000). We use the  
149 term ‘agglutinated’ to describe clasts that have stuck together on deposition. We use the term

150 'welded' to describe scoria and spatter deposits in which clasts have agglutinated and have  
151 subsequently partially to totally lost their outlines and undergone a strong degree of compaction  
152 flattening. The term 'clastogenic lava' is reserved for a flow composed of partially coalesced  
153 pyroclasts. We have divided the Roza pyroclastic deposits into different classes dependent on  
154 average bulk rock densities, clast aspect ratios and grainsize (Table 1).

155 At most localities where the base of the Roza pyroclastic deposits is visible, they overlie  
156 pāhoehoe lavas of the Roza Member. Below we describe the most instructive and best-exposed  
157 outcrops of pyroclastic deposits associated with each vent segment, from north to south, in terms of  
158 their stratigraphy, geometry and lithofacies associations. We also describe the Roza lavas that buried,  
159 and led partially to the preservation of, the pyroclastic deposits. Useful details from poorer quality  
160 outcrops are summarised in Table 2.

161

#### 162 *Buffalo Spring North (BSN)*

163 The Buffalo Spring North vent construct lies 900 m south-southeast of the northernmost exposed  
164 Roza vent accumulations (the poorly exposed Harder Ranch vent; Fig. 1B, Table 2). It is an eroded  
165 pyroclastic edifice comprised of weakly to densely agglutinated scoria and spatter and lava-like  
166 densely welded spatter (Table 1 and Fig. 4B) exposed over 0.3 km<sup>2</sup>. Bedding and agglutination  
167 fabrics dip 6–35° to the SW, W and NW and define the western side of an edifice with an apparent  
168 radius of >330 m and a minimum length of 560 m (Fig. 4B, Table 3). The bulk of the exposed  
169 pyroclastic deposits are densely agglutinated scoria and spatter (lithofacies dwScL, dwSpB) and  
170 lava-like densely welded spatter (lithofacies llwSp; Fig. 2D-F) in beds several decimeters to several  
171 meters thick. Spatter bombs within the deposits reach 1 m in diameter. Rheomorphic flow of some  
172 lava-like spatter beds is indicated by brecciated vesicular layers and centimeter-scale tension gashes.

173

#### 174 *Buffalo Spring South (BSS)*



175 Pyroclastic deposits of the Buffalo Spring South vent construct outcrop 700 m south-southeast of the  
176 BSN and cover 0.06 km<sup>2</sup> (Fig. 4A and C). Dips of beds (or bedding planes) vary from 8–31°, with an  
177 average ~ 16° and define the NE, E and SE portions of a small volcanic edifice. The edifice is  
178 elongated in a NW–SE direction and the preserved (exposed?) part has a radius of 130 m and a  
179 length of 280 m (Table 3). Inward-dipping strata define the position of the crater, while the SW  
180 portion of the cone passes into an area of non-systematic dips and strikes (Fig. 4C). The NW portion  
181 of the construct is not preserved. The edifice is comprised of bedded moderately and densely  
182 agglutinated scoria lapilli and spatter. The stratigraphically oldest deposits exposed are black, lava-  
183 like densely welded spatter. Vesicular spatter bombs are conspicuous and reach 1 m long and are  
184 common within beds of oxidised moderately agglutinated scoria (e.g., Fig. 3C). The bombs have  
185 aspect ratios of 1:2–1:10 and are non- to moderately vesicular (<55 vol. %) and typically have black  
186 interiors and brown, altered glassy exteriors with ropy and fluidal textures.

187

#### 188 *Rock Creek Center (RCC)*

189 A > 50 m-thick sequence of pyroclastic deposits is exposed along the eastern bank of Rock Creek  
190 (Fig. 5). The succession drapes a series of earlier Roza sheet lobes that vary in thickness from 10 m  
191 in the north to 25 m in the south, over a distance of 400 m (Fig. 5A). The pyroclastic succession  
192 consequently thins to the south over the lavas and appears to merge with the pyroclastic deposits of  
193 the RCE vent (Fig. 5A). The sheet lobes are the oldest Roza products exposed in Rock Creek and  
194 they locally pass upwards into 3 m of lava-like densely welded spatter and thin clastogenic lava  
195 flows (Fig. 6). This is overlain by a 1.5 m thick lithic breccia comprised of angular blocks and  
196 boulders, and of densely welded Roza spatter, similar to the underlying deposits (Fig. 6). The lithic  
197 blocks and boulders are composed of Roza lava. This is overlain by a well-sorted 2 m-thick scoria  
198 fall deposit that gradually fines upwards. The upper meter of the fall deposit is densely welded  
199 without any observable increase in grainsize. This would suggest an increase in accumulation rate

200 during deposition of this welded part of the bed. This is sharply overlain by 6 m of clastogenic lava  
201 and vitrophyric spatter (Fig. 6). The upper ~ 35 m of the succession is dominated by red oxidised  
202 weakly and moderately agglutinated scoria (ScL and waScL, Table 2) in massive or diffusely bedded  
203 units that range in thickness from < 1–15 m thick. Thinner intercalated agglutinated beds (waScL;  
204 Table 1) typically show poorly developed columnar joints. Beds in this succession dip 10–22° to the  
205 north, east and west and define a half cone with an estimated minimum radius of 250 m and a  
206 minimum length of 430 m (Fig. 5C and Table 3). The vent that emitted these pyroclastic deposits is  
207 inferred to sit under Rock Creek and is probably aligned NNW–SSE (Fig. 5).

208

#### 209 *Rock Creek East (RCE)*

210 Pyroclastic deposits of the Rock Creek East vent outcrop over 1.15 km<sup>2</sup> of channelled scabland to the  
211 east of the track that leads into Rock Creek (Fig. 1 and 5D). At the southeastern end bedding dips  
212 and strikes outline a pyroclastic edifice estimated to be ~400 × 500 m in diameter (Fig. 5D, Table 3).  
213 The center of the edifice is cut by a 70 m-wide channel filled with alluvial sediments: we infer that  
214 this is coincident with the position of the vent around which the edifice was constructed. Beds dip  
215 13–44° east and north. Less well-exposed pyroclastic deposits dip 10–21° to the south on the  
216 southern flank of the edifice (Fig. 5B). Lower parts of the northern and southern flanks of the edifice  
217 are comprised of black lava-like and densely welded spatter. This passes up into lower grade  
218 densely-welded and moderately agglutinated scoria and densely welded spatter that makes up the  
219 bulk of the preserved northern flanks (Fig. 5B). There are several small outcrops of densely welded  
220 spatter in the channel that dip inwards at steep angles (44–65°): these are inferred to be deposits that  
221 have slumped into the vent (not exposed) or that mantled the steep interior crater walls of the edifice.  
222 Later-emplaced Roza sheet lobes onlap against the cone and completely cover it to the south;  
223 discordant relationships between steeply dipping strata and horizontal sheet lobes on the east side of  
224 the vent indicate that the crater was also inundated by lava.

225        Bedded pyroclastic deposits extend 500 m to the north of the edifice and outcrop over an area  
226 of 0.15 km<sup>2</sup>. Dips and strikes of bedding and welding fabrics are non-systematic and change rapidly  
227 (Fig. 5D). Dips vary from 0–60° in all directions but do not outline obvious cones or partial cones.  
228 Individual beds cannot be traced laterally due to rapid changes in dip and strike, limited exposure,  
229 and rapid changes in agglutination intensity. Vents have not been recognised in this area and we infer  
230 that the pyroclastic deposits were erupted from the same vent that constructed the cone to the south,  
231 thus were dispersed up to 700 m from this vent area.

232        It is of interest to note that the vent that fed RCE appears to lie ~1 km east (orthogonal to  
233 fissure axis) of the vent that fed RCC (Fig. 5A), suggesting an en echelon arrangement of fissures.

234

#### 235 *Texas Draw (TD)*

236        The Texas Draw vent area (Fig. 1 and 7) is marked by bedded weakly to densely agglutinated scoria  
237 and spatter exposed over an along-fissure distance of 1 km and an area of >1.6 km<sup>2</sup>. The base of the  
238 pyroclastic succession is not seen. In northern areas, bedding and welding fabric orientations define  
239 an edifice with slopes generally dipping 16–34° to the north, west and south (Fig. 7A, B and E). We  
240 infer that this edifice was constructed on the western side of a ~N–S-trending vent that ran down the  
241 valley. An eastern counterpart to this edifice is missing and post-pyroclastic phase lavas are instead  
242 exposed (Fig. 7B). In detail the dips and strikes within this edifice are complicated. Dip direction and  
243 magnitude change rapidly over distances of 10's of meters and define significant smaller-scale  
244 topography (Fig. 7B). A 60 m-wide depression demarcated by inward-dipping beds is present on the  
245 inner side of the edifice at the north and may represent a slump scar mantled by pyroclastic fall  
246 deposits (Fig. 7A). Up to 30 m thickness of continuous pyroclastic deposits are exposed at the  
247 southern end of the edifice (Fig. 7C). The lower 15 m comprises bedded brown to red weakly to  
248 densely agglutinated bedded scoria with large spatter bombs (< 40 cm in diameter, Fig. 7C).  
249 Moderately agglutinated scoria beds tend to form discontinuous lenses 5–50 cm thick and up to 5 m

250 wide. This passes upwards into a succession dominated by densely agglutinated scoria and spatter.  
251 Several thick beds of densely agglutinated scoria are persistent over hundreds of meters and exhibit  
252 columnar joints spaced ~ 10–50 cm apart. The upper ~ 15 m consists of higher grade pyroclastic  
253 deposits (densely agglutinated scoria and spatter and lava-like densely welded spatter), in beds from  
254 < 1m to > 5 m thick. Changes in welding grade are abrupt (Figs 6 and 7) and individual pyroclastic  
255 fall layers pinch out or change character (e.g., in degree of agglutination) markedly over lateral  
256 distances of several 10's–100's of meters (Fig. 7).

257 To the south and southeast of the edifice, dips and strikes are much less systematic and  
258 individual edifices are more difficult to define. The exposed thickness of the pyroclastic deposits  
259 exceeds 10 m in places and dips vary from 0–45° and change magnitude and direction rapidly.  
260 Several ridges with broadly opposing dips are present (Fig. 7B) but there is no direct evidence for  
261 vents or craters. The complicated nature of the Texas Draw outcrops suggests that the pyroclastic  
262 deposits may be the products of more than one sub-parallel or en echelon vents.

263 The pyroclastic beds are partially overlain by columnar jointed Roza sheet lobes (Fig. 7A and  
264 B), of which typically only the cores are exposed (upper crusts have been eroded and bases are not  
265 seen).

266

#### 267 *Mason Draw (MD)*

268 Pyroclastic deposits at Mason Draw (Fig. 1) are exposed over an area of at least 5 km<sup>2</sup>. Most  
269 outcrops are small (several meters wide), of poorer quality than those described above and comprise  
270 moderately to densely agglutinated scoria and spatter outcropping over 2.6 km<sup>2</sup>. The base of the  
271 pyroclastic deposits and of the Roza Member is not exposed. Bedding dips and fabrics dip 10–27° to  
272 the S, SW and NW and define an edifice similar to that at Texas Draw. This edifice is elongated  
273 approximately north-south. Consistent westward dips suggest that the edifice had a radius of 500 m  
274 and a length of >500 m. We infer that it built up around a vent located beneath the present valley

275 floor. The western rim lacks an eastern counterpart and Roza sheet lobes outcrop at the same  
276 stratigraphic level on the other side of the valley. The cone (or spatter rampart) passes westward and  
277 northward into variably agglutinated pyroclastic deposits that, as at other vents, exhibit non-  
278 systematic and rapidly changing dips and strikes. Locally, steeply-dipping densely welded spatter  
279 beds record slumping of hot pyroclastic deposits. The edifice is overlain by Roza sheet lobes to the  
280 north, although horizontal-bedded pyroclastic deposits are exposed 500 m north of the edifice (Fig.  
281 1). Wedges of weakly to moderately welded scoria and densely welded spatter occur on top of Roza  
282 sheet lobes NE of the Mason Draw vent deposits.

283

#### 284 *Winona (WI)*

285 Pyroclastic deposits representing the Winona vent accumulations (Fig. 1) are primarily exposed in  
286 discontinuous, but in total 3 km-long, east-west trending road and railroad cuts. This set of exposures  
287 provides a section through a vent and examples of pyroclastic fall deposits inter-bedded with thin  
288 pāhoehoe lavas. Both the fall deposits and the lavas are inferred to have been sourced at the vent.  
289 The lowermost exposed products of the Roza Member in the Winona area are pāhoehoe lobes with  
290 thick rubbly, highly vesicular upper crusts and dense, columnar jointed cores. They are best exposed  
291 in man-made sections in roads as small lobes several meters to several 10's m wide and up to 8  
292 meters thick (Fig. 8A and B). The upper crust on these lobes is up to 5 meters thick, indicating  
293 emplacement times of ~6 months (Hon et al., 1994). The upper surfaces of these lavas in one area  
294 exhibit tumuli spaced >10 meters apart with relief of several meters. Source vents for these early  
295 Roza lobes in this area are not known.

296 Rail cuts west of Winona, that parallel the south bank of the Palouse River provide a cross-  
297 section through the vent system, which here consists of two opposing mounds of outward-dipping  
298 densely agglutinated spatter (Fig. 8B). The western mound comprises > 10 m of densely welded  
299 spatter (Fig. 8C) that dips 5° towards the east and is exposed for 140 m along the railway track. It

300 has a wedge-like morphology in cross-section and tapers to the east. The base and top of this spatter  
301 unit are not exposed but the grade of welding decreases upwards and also decreases eastwards,  
302 although exposure is broken. The mound has a steep eastern margin that abuts against two columnar  
303 jointed Roza sheet lobes (Fig. 8B). The sheet lobes sit within a 160 m wide depression that is bound  
304 on its western margin by a westward tapering mound, ~400 m wide, of densely welded and lava-like  
305 spatter similar to that already described. Welding fabric within this second wedge dips  $7^\circ$  to the west.  
306 We infer that these two wedges constitute a low-profile spatter cone constructed either side of a vent  
307 that subsequently filled with Roza lava. Vertical welding fabrics are present within some parts of  
308 these wedges and may have formed during slumping or mantling of crater walls. Mounds of weakly  
309 to moderately agglutinated scoria and densely welded spatter outcrop on top of a Roza sheet lobe  
310 over a wide area at the western end of the railway section at Winona (rafted spatter on Fig. 8A).  
311 Adjacent mounds show diverging bedding and welding fabric dips, however the continuation of the  
312 deposits in 3D is not known.

313 Well-sorted scoria fall deposits outcrop at several places around Winona. At the eastern end  
314 of the railway section, and in road cuts 1.7 km to the east of the vent, at the same stratigraphic  
315 horizon as the densely welded spatter mounds, is an ~8 m thick sequence of scoria fall deposits and  
316 vesicular rubbly lavas (see Thordarson and Self, 1996, 1998). Overlying the lowermost Roza lavas  
317 are two clast-supported, well sorted scoria fall deposits separated by a vesicular rubbly pāhoehoe  
318 lobe. The fall deposits are each  $> 2$  m thick and are un- to moderately altered. The fall deposits are  
319 massive apart from several thin (5–6 cm thick) finer-grained horizons. Where unaltered they  
320 comprise well-sorted black scoria lapilli up to 5 cm in diameter. The scoria lapilli have densities of  
321  $300\text{--}1100\text{ kg m}^{-3}$ , equivalent to vesicularity values of 65–90 vol. % (Fig. 9C). Modal values are 500–  
322  $600\text{ kg m}^{-3}$  (80–84 %). Clasts exhibit numerous small spheroidal vesicles (Fig. 3A) and have fused  
323 exteriors and fractured surfaces (Thordarson and Self, 1998). The Roza fall deposit is in its physical  
324 properties very similar to the tephra from the explosive phases of sub-Plinian intensities produced by

325 the 1783-84AD and 934-40 AD Eldgjá flood lava eruptions (e.g. Thordarson and Self, 1993;  
326 Thordarson et al., 2001). Clast morphologies (including achenliths) and vesicularities (between 75-  
327 90 vol% in all cases) are comparable and so is the grainsize distribution of the proximal tephra (Fig.  
328 9D). We infer that these fall deposits coarsen eastward into the densely agglutinated spatter mounds  
329 at the Winona vent, 1.7 km to the west. The scoria fall deposits under and above the rubbly lava have  
330 been disrupted into a series of meter-scale mounds ('pumice ramparts' of Swanson et al., 1975) by  
331 continued movement of the lava beneath during and immediately post deposition.

332 Correlating fall deposits across the region is difficult due to the monotonous nature of their  
333 physical characteristics, the weak, locally absent bedding, the rapid lateral facies changes close to  
334 inferred vents, and the intercalated pāhoehoe lavas that diachronously dissect the deposit and are  
335 themselves not possible to correlate between outcrops. The upper contact of the fall deposit is  
336 invariably welded to a depth of 5–15 cm, and commonly thermally discolored (oxidised) to a depth  
337 of a meter or more, and exhibits ~ 10 cm-spaced curving columnar joints as well as thermal  
338 discoloration. The density of the fall deposits increases up through the welded zone from 950 kg m<sup>-3</sup>  
339 to 1550 kg m<sup>-3</sup> over 35 cm. In the thicker sections of the fall deposits it is not uncommon to find  
340 intercalated thin spongy pāhoehoe lobes; these are typically less than a meter thick. At some  
341 locations the fall deposit grades down into > 5 m of coarse-grained non- to moderately-agglutinated  
342 scoria with coarse bombs.

343

#### 344 *Post-pyroclastic-deposit lava flows*

345 The pyroclastic edifices along the Roza vent system are overlapped by 1–5 horizontal Roza sheet lobes  
346 (e.g., Figs. 4 and 5). These lobes are typically between 1–20 m thick, with classic tripartite lower  
347 crust, core and upper crust divisions of pāhoehoe lavas (Thordarson and Self, 1998). The upper  
348 crusts of these sheet lobes are widely in excess of 6 m thick and are defined by decimeter to meter  
349 thick diffuse vesicle bands. Emplacement times for these lobes are in the order of 9–12 months

350 (based on empirical model of upper crust growth of Hon et al., 1994; see also Thordarson and Self,  
351 1998). It seems probable that only the largest edifices of pyroclastic deposits remained unburied by  
352 Roza sheet lobes. At the base of some sheet lobes are packages of centimeter- to decimeter-thick  
353 vaguely defined vesicular pāhoehoe lobes with thin glassy and partially annealed crusts. These  
354 packages can reach several meters thick. Gas blisters up to 70 cm high occur beneath crusts in some  
355 sheet lobes. The southern end of the Mason Draw edifice is overlain by several meters of thin,  
356 spongy and shelly pāhoehoe lobes. Shelly pāhoehoe consists of lobes that are < 50 cm thick, < 1 m  
357 wide and have large gas cavities beneath the thin crusts. Rafted mounds of moderately and densely  
358 agglutinated spatter occur on top of sheet lobes to the NW of the edifice.

359 At several off axis locations along the fissure (e.g., western end of Winona railcut, Fig. 8A  
360 and B) small mounds of rafted variably oriented weak to moderately welded and agglutinated scoria  
361 overlie the upper sheet lobes. The upper surface of the lava must have exhibited considerable relief  
362 (2–4 m) as meters-thick beds of scoria and spatter occur at the same level as exposed sheet lobe  
363 cores. Bedding defined by fabrics in these pyroclastic deposits dips non-systematically. At one  
364 locality, it appears that the bedded spatter and scoria drape 5 meters of relief on the margin of a sheet  
365 lobe.

366

## 367 **Interpretation**

### 368 *Spacing of pyroclastic cones along the Roza fissure*

369 At least 11 separate vents have been identified from surface pyroclastic deposits over a distance of ~  
370 32 km (Fig. 1). The spacing of large Roza pyroclastic cones is 0.8–4 km, with an average of 2 km.  
371 The average spacing of large cones along the Roza fissure is similar to that along the 27 km-long  
372 Laki fissure, Iceland, where large pyroclastic constructs are spaced 0.5–5 km apart (average 1.5 km;  
373 Thordarson and Self, 1993). Incomplete exposure and the burial of pyroclastic deposits by later-  
374 erupted Roza lavas, plus parts of the fissure covered by younger sediments, including loess, inhibit a



375 full understanding of the number and spacing of vents along the fissure. At Laki, pyroclastic cones  
376 and spatter ramparts occur nearly continuously along the entire length of the fissure; 70 separate  
377 vents were active along the 4.5 km-long fissure during the 1983 eruption of Miyakejima (Aramaki et  
378 al., 1986). However, the similarity in terms of vent spacing and cone dimensions between the Roza  
379 and the Laki eruptions suggests overlap in physical processes and that Laki makes a reasonable first-  
380 order analogue in this respect for the Roza vent system. The Roza agglutinate cones may have  
381 lithological similarities to the proximal deposits of the 934 AD Eldgjá eruption on Iceland  
382 (Thordarson et al., 2001).

383         The position of the vents along the Roza fissure is precisely known, but large discrete  
384 outcrops of densely agglutinated spatter and coarse spatter bombs occur over zones up to 1–4 km  
385 wide orthogonal to the trend of the fissure (e.g., Winona and Rock Creek, Fig 1B). This suggests that  
386 activity may have occurred locally from several sub-parallel overlapping fissure segments (e.g., Fig.  
387 5) spread across a zone up to several kilometres wide. This is unusual compared with historic fissure  
388 eruptions which have come from very narrow zones,  $\ll$  1 km (e.g., Miyakejima volcano, Japan,  
389 Aramaki et al., 1986; Laki, Iceland, Thordarson and Self, 1993).

390

#### 391 *Reconstruction of proximal pyroclastic constructs*

392 A range of edifice constructs are present along the Roza fissure, from broad, probably lava-  
393 dominated (but very poorly exposed) cones/shields (e.g., Big Butte and Little Butte, Table 2),  
394 through to pyroclastic edifices composed dominantly of agglutinated spatter and scoria (e.g., BSN,  
395 BSS, RCC, RCE, TD, MD and WI). It is the latter upon which we focus this discussion. The  
396 pyroclastic edifices are composed of a range of pyroclastic deposits. The characteristics of the Roza  
397 pyroclasts, including the coarse grainsize, abundant fluidal-shaped clasts, scoriaceous clasts, spatter  
398 bombs, achneliths (Pele's tears) (Table 1 and Fig. 2) are typical products of strong gas-driven fire  
399 fountain activity in basaltic eruptions of all scales. Proximal pyroclastic sedimentation is inherently

400 unsteady (e.g., Head and Wilson, 1987; Houghton et al., 2004) and fluctuations in gas content,  
401 pyroclast grainsize, accumulation rate, and fountain height, structure, orientation and temperature  
402 can result in complex lateral and vertical sequences of pyroclastic deposits. Such unsteadiness  
403 accounts for the abrupt vertical and lateral changes in agglutination state and grainsize within the  
404 Roza proximal deposits (see Figs. 6 and 7). Beds of densely agglutinated scoria commonly show  
405 columnar joints (e.g., Fig. 2) indicating that they were emplaced rapidly and then cooled as single  
406 units. Closely-spaced platy jointed units at the base of some lava-like densely welded spatter are  
407 similar to those at Pu‘u ‘Ō‘ō, Kilauea, interpreted by Heliker et al. (2003) as shear planes beneath  
408 clastogenic lava flows.

409         The radii of preserved Roza pyroclastic edifices, orthogonal to the inferred axis of the fissure  
410 vent system, are > 200–400 m and their lengths parallel to the fissure are > 280–900 m. Around most  
411 Roza vents bedding dips of pyroclastic deposits and dips of welding fabrics are in the range 4–34°,  
412 with mean values of 15–19° (Fig. 9A). The deposits crudely define partial cones with outward radial  
413 dips over sectors of <180°. Geometric reconstructions using these dimensions and the dips of  
414 bedding planes and welding fabrics give restored edifice heights of 15–160 m (Table 3) and volumes  
415 of pyroclastic cones in the range of  $10^{-4}$  to  $10^{-2}$  km<sup>3</sup>. If we assume that cones, both small (50%) and  
416 large (50%), are spaced 1 km apart along the 300 km-long Roza fissure, then a minimum volume of  
417 pyroclastic material preserved as cones is ~ 10 km<sup>3</sup> (< 3–5 km<sup>3</sup> DRE). We infer that an equivalent  
418 volume was dispersed widely as ash and scoria fall deposits during the eruption. This is equivalent to  
419 < 1% of the total erupted volume of the Roza Member. We refer to these cones as ‘agglutinate cones’  
420 to distinguish them from scoria cones and spatter cones.

421         Many of these agglutinate cones appear to be elongated in N–S or NNW–SSE directions  
422 (Table 3), which is consistent with the overall trend of the Roza vent system. Several appear to have  
423 built up preferentially on one side of the inferred vents with opposite parts missing (e.g., TD, MD  
424 vents). Their absence could be due to deposition from strongly wind-sheared plumes, from

425 deposition from angled fountains, or from the rafting away of large sectors of the cone on top of lava  
426 flows. Evidence for rafting is seen at Mason Draw, Winona and Palouse River vents (Fig. 1). Around  
427 several of the vents the pyroclastic edifices pass laterally into extensive areas where bedding  
428 orientations are non-systematic and change rapidly in dip and strike (e.g., RCE, TD and MD vents).  
429 These regions cannot easily be explained as areas where neighbouring cones converged and  
430 overlapped (as is common along fissures, Thordarson and Self, 1993; Sable et al., 2006) because dips  
431 are extremely variable. Instead, such areas are consistent with the draping of irregular topography  
432 (formed by subjacent sheet lobes and hummocky pāhoehoe flows) by sheet-form welded and  
433 agglutinated fall deposits. At Rock Creek Center these deposits extend up to 750 m away from the  
434 vent (Fig. 5); at Mason Draw they extend > 500 m from the vent.

435         Few of the agglutinate cones preserve crater deposits. Steep, inward-dipping strata at Rock  
436 Creek East and Buffalo Spring South are inferred to be agglutinated spatter that is either mantling  
437 crater walls or has slumped into the crater or vent (Figs 4 and 5). Several poorly exposed crater  
438 deposits outcrop south of the Snake River (e.g., Potter White Hill and Crow Creek, Table 2). These  
439 comprise lithic clast-rich agglutinate breccias and densely agglutinated spatter. They show evidence  
440 for slumping and commonly have steep contacts between adjacent pyroclastic units.

441         The dimensions of the Roza agglutinate cones are comparable to scoria cones formed during  
442 both small monogenetic basaltic eruptions (e.g., Porter, 1972; Wood, 1980) and larger basaltic  
443 fissure eruptions (e.g., cones along the 1783–5 Laki fissure eruption, Iceland, Thordarson and Self,  
444 1993). However, the Roza edifices differ from scoria cones in two important ways. First, they are  
445 composed dominantly of welded and agglutinated spatter and scoria, even at distances of > 400 m  
446 from the vent. Loose, non-welded/agglutinated scoria deposits account for only a small volume of  
447 the preserved cones—the edifice at the Rock Creek Center vent has the thickest succession of low-  
448 grade pyroclastic material with >30 m of weakly to non-welded scoria (ScL, waScL; Fig. 6).  
449 Typically non-welded/agglutinated pyroclastic deposits are absent or account for only a small

450 volume of each edifice. It is not the case that overlying loose accumulations of typical scoria cone  
451 deposits have been eroded because later Roza onlap onto these edifices at several locations (e.g.,  
452 RCE, RCC, TD, MD and WI). Thus, in many instances the preserved deposits more or less represent  
453 the entire pyroclastic construct. Second, the mean dips of beds and welding fabrics in the Roza  
454 edifices (Fig. 9A) are considerably lower than those typical of scoria cones, which are commonly at  
455 the critical angle of repose for loose scoria as a result of grainflow ( $\sim 35^\circ$ , Wood, 1980). These two  
456 characteristics set apart the Roza edifices from most pyroclastic cones constructed during basaltic  
457 eruptions, and are indicative of phases of vigorous fountaining. Fountains during Hawai‘ian  
458 eruptions typically range from 100–500 m in height, spatter-rich accumulations are commonly  
459 limited to ultra-proximal regions and spatter cones typically extend only meters to tens-of-meters  
460 from vents and may reach a few 10s of meters high (e.g., Thordarson and Self, 1993; Parcheta et al.,  
461 2012).

462 Individual fall layers are not traceable away from the Roza vents and thus isopach maps  
463 cannot be constructed with which to extract quantitative measures of pyroclast dispersal (e.g.,  
464 thickness half-distance,  $b_t$ , Pyle, 1989). In the absence of this information a useful measure is the  
465 linear thickness half-distance — the distance over which a fall deposit halves in thickness away from  
466 source ( $t_{1/2}$ , Houghton et al., 2004). For example, linear thickness half-distance values for Hawaiian-  
467 Strombolian cones are 6–30 m (Sable et al., 2006). These values can be calculated crudely for  
468 packages of Roza fall deposits that constitute the remnant cones by using the geometric and  
469 structural data in Table 3. Roza fall deposits have  $t_{1/2}$  values of  $\sim 110$ –200 m. This, of course, bundles  
470 together fall deposits that may have widely varying  $t_{1/2}$  values, that show varying degrees of welding  
471 or agglutination, and that may include clastogenic lava flows, so they must be interpreted with care.  
472 Such  $t_{1/2}$  values are comparable to those from the more widely dispersed proximal fall deposits from  
473 the 1886 basaltic Plinian eruption of Tarawera, New Zealand (Sable et al., 2006).

474

475 **Discussion**

476 *Fountain and eruption dynamics*

477 The unusual characteristics of the Roza edifices, defined by widespread agglutinated and welded  
478 deposits, low to moderate slope angles, and  $t_{1/2}$  distances of 110–200 m, suggest deposition from tall,  
479 vigorous fountains and sustained convection columns (Fig. 10). The evidence suggests that the  
480 intensity of eruptions at Roza vents was periodically much higher than is typical for effusive basaltic  
481 eruptions. For example, the maximum heights of fire fountains on Hawai‘i are commonly <500 m,  
482 occasionally reaching 800 m (e.g., Wolfe et al., 1988; Sparks et al., 1997): a 400 m-high fountain  
483 typically has a basal diameter of <150 m. Fountains of this height only sustain weak convective ash-  
484 laden plumes, and the cones that form around them are composed predominantly of loose scoria  
485 clasts (e.g., the Pu‘u ‘Ō‘ō cone, Hawai‘i, Heliker et al., 2003). Deposits from higher intensity  
486 basaltic eruptions include those of the 1886 eruption of Tarawera, New Zealand (Walker et al., 1984;  
487 Sable et al., 2006). The  $t_{1/2}$  values of some of the Tarawera deposits compare well with those of the  
488 Roza: Sable et al. (2009) interpreted them as a result of sedimentation from low portions (1–4 km  
489 height) of buoyant Plinian columns (lower convective regions and momentum driven jet regions) as  
490 the pyroclast release heights were greater than those typically reached by lava fountains or  
491 Strombolian eruptions. Abnormally high lava fountains (1.6 km) during the 1986 basaltic andesite-  
492 basaltic eruption of Izu-Oshima volcano, Japan, fed a Subplinian plume that reached 16 km high  
493 (Sumner, 1998; Mannen and Ito, 2007). During the 1783–5 eruption of Laki, Iceland, fountains  
494 reached 0.8–1.4 km in height and produced Subplinian columns of up to 15 km height. High  
495 fountains have been invoked to account for the occurrence of rheomorphic lava and densely to  
496 poorly welded spatter deposits up to 1.5 km from the vents of the Biskupsfell fissure eruption at  
497 Kverkfjöll, Iceland (Karhunen, 1988).

498 High pyroclast accumulation rates (> 20 cm/min) are needed to cause pyroclasts to weld and  
499 agglutinate on deposition (Sparks and Wright, 1979; Thomas and Sparks, 1992). Sable et al. (2006)

500 calculated average accumulation rates of 15–20 cm/minute for the mostly non-welded Tarawera  
501 deposits (see also Walker et al., 1984). These are comparable to the 17 cm/min average accumulation  
502 rates of the cone-building phase of the 1986 eruption of Izu-Oshima volcano, Japan (Sumner, 1998).  
503 For the Roza eruptions these rates must have been achieved and exceeded at distances of up to 500 m  
504 from the vent for extended periods. In order to achieve this the Roza fountains needed to be high (>>  
505 1 km) and sedimentation from the fountains needed to be enhanced by fallout of coarse, hot  
506 pyroclasts from the lower parts of associated convecting plumes of potentially Subplinian to Plinian  
507 intensity (e.g., Thomas and Sparks, 1992; Sable et al., 2009). Average accumulation rates of ~ 20  
508 cm/min would give construction durations of up to 5–13 hours for Roza cones, which are comparable  
509 to the estimated durations of basaltic Plinian and Subplinian eruptions elsewhere (e.g., Sable et al.,  
510 2006; see Houghton and Gonnermann, 2008).

511       The thick sheet-form scoria fall deposits preserved at distances of > 0.1–1.7 km from the  
512 Roza vents are interpreted as the products of the sustained plumes developed above the fountains.  
513 Poor lateral exposure makes it difficult to correlate individual scoria fall deposits and isopach maps  
514 cannot be constructed; intercalated pāhoehoe lobes at many localities further complicate the  
515 stratigraphy. The massive to weakly bedded nature of the deposits indicates deposition from semi-  
516 sustained, quasi-steady, pulsating plumes (rather than intermittent Strombolian eruptions). At  
517 Winona individual fall layers reach > 2 m thick at > 1.5 km from source. These deposits and the  
518 characteristics of the pyroclasts are comparable to documented basaltic Subplinian and Plinian fall  
519 deposits elsewhere (e.g., Walker et al., 1984; Thordarson and Self, 1993; Costantini et al., 2009,  
520 2011), however there are insufficient outcrops to construct isopach maps and constrain their  
521 dispersal.

522       Whilst welded and agglutinated fall deposits occur in the proximal deposits of all of the  
523 modern examples highlighted above, they are not as dominant or as widespread as in the Roza  
524 example (cf. Sable et al., 2006), and we have yet to find documentation of comparable volcanic

525 edifices in the literature. We interpret this to mean that eruptions at the Roza vents were periodically  
526 characterised by eruptions with unusually vigorous, tall fountains that were most probably topped by  
527 sustained and tall convective columns (Fig. 10). These may have been comparable to other  
528 documented examples (e.g., Tarawera, Laki and Izu-Oshima eruptions). Explosive basaltic eruptions  
529 of Subplinian scale or larger have received a lot of interest recently, (Houghton et al., 2004; Sable et  
530 al. 2006; Vergnolle and Caplan-Auerbach, 2006; Constantini et al., 2009, 2011) but there is much  
531 that remains unknown (see review in Houghton and Gonnermann, 2008). The geometry and  
532 lithology of the Roza edifices are compatible with growth during eruptive phases of substantially  
533 higher intensity than is normally associated with lava-dominated basaltic eruptions (i.e, that of  
534 typical Hawaiian-Strombolian activity). Controls on the explosivity of basaltic eruptions have been  
535 linked to bubble rise and coalescence, degassing processes and melt rheology driven by microlite  
536 crystallisation (Houghton and Gonnermann, 2008). An in-depth discussion of the parameters  
537 controlling more vigorously explosive phases of the Roza eruption is beyond the scope of this paper  
538 and will be dealt with in a future publication.

539

#### 540 *Eruption scenario at a Roza vent*

541 The Roza fissure is considered to have unzipped from the south to the north based on the  
542 geochemical stratigraphy of the stacked sheet lobes in the lava flow field (Martin, 1989). Lavas  
543 flowed north and west (until the last phase of the eruption) inundating the paleo-surface in advance  
544 of the propagating fissure segments. The base of the Roza Member is rarely exposed north of the  
545 Snake River and is not seen at any of the outcrops exposing pyroclastic material; the inference is that  
546 activity at several vents appears to have taken place through earlier-emplaced Roza lavas. At  
547 Winona, Rock Creek and Union Flat Creek (Fig. 1) the pyroclastic deposits overlie Roza lava  
548 indicating that the area was already partially inundated by hummocky pāhoehoe flows. At Rock  
549 Creek (Fig. 5) the oldest exposed Roza lavas pass upwards into clastogenic lava and densely welded

550 spatter. We infer that these fountain-fed clastogenic lavas came from the Rock Creek vent during  
551 early phases of the eruptions.

552 Explosive pyroclastic eruptions seemed to have occurred early on at each vent. This vigorous  
553 activity shed clasts from tall fountains and from the lower parts of convective columns and built-up  
554 broad cones composed of moderately to densely agglutinated scoria and spatter and lava-like densely  
555 welded spatter that extended > 750 m away from the vent (Fig. 10). Buoyant plumes above vigorous  
556 fountains dispersed scoria and ash away from the vents. Numerous closely-spaced vents for  
557 explosive activity along the fissure led to the convergence and overlap of pyroclastic deposits,  
558 building up complex proximal agglutinate cone morphologies and stratigraphies (cf. Thordarson and  
559 Self, 1998). Rootless lavas flowing away from the bases of the fountains periodically breached the  
560 growing cones and rafted sectors of them away. Based solely on probable minimum accumulation  
561 rates, each of these periods of high intensity activity lasted for > 5 to 13 hours at each vent. However,  
562 the pyroclastic material preserved in the edifices constitutes only a very small fraction (< 1 %) of the  
563 erupted mass: a much greater mass may have been emplaced as clastogenic lavas during these high  
564 intensity phases because much material falling at high accumulation rates rapidly coalesces and  
565 flows away from the vent, as seen at Laki (Thordarson and Self, 1993). Thus, these phases may have  
566 been longer-lived and we cannot constrain how many of these phases there were during the Roza  
567 eruption. Through a lack of evidence to the contrary we presently favor a scenario where the bulk of  
568 the mass of the Roza Member was effused by long-lived, low intensity fountains. The whole Roza  
569 eruption lasted for years to perhaps several decades (Thordarson and Self, 1998) and during this time  
570 inflating sheet lobes partially to totally buried the pyroclastic edifices.

## 572 **Conclusions**

573 The 15 Ma Roza Member has the best exposed vent system and associated pyroclastic deposits of  
574 any flood basalt flow field. Investigations of its proximal pyroclastic deposits reveal that the



575 eruptions constructed unusual, broad edifices, here termed agglutinate cones, composed mostly of  
576 moderately to densely agglutinated spatter and scoria. Temporal and spatial changes in fountain  
577 structure, clast temperature and clast accumulation rate are recorded by complex and rapid facies  
578 changes in the deposits that constitute the cones. These edifices have minimum radii of 200–500 m  
579 and minimum reconstructed heights of 15–160 m, and may represent a new type of basaltic  
580 pyroclastic edifice not previously documented in the literature. The recorded volcanic activity does  
581 not fit with presently known eruption styles of basaltic magmas and we infer that the cones were  
582 constructed during unusually vigorous explosive phases. Clasts fell out of tall ( $>> 1$  km-high)  
583 fountains as well as from the margins of the lower portions of strongly convective columns. Well  
584 sorted, highly vesicular scoria lapilli and ash fell out from umbrella regions of these columns. These  
585 explosive phases are interpreted to have been relatively short-lived phenomenon that may have  
586 emplaced only a fraction ( $>10 \text{ km}^3$  DRE) of the total erupted mass of the Roza Member. As well as  
587 providing the first detailed descriptions of flood-basalt proximal vent edifices and deposits, the  
588 outlined geological evidence suggests that the Roza eruption was periodically and repeatedly capable  
589 of injecting climate-altering gases high into the atmosphere.

590

## 591 **Acknowledgements**

592 This research was funded by NERC standard grant NE/E019021/1 awarded to SS at The Open  
593 University. RJB thanks Linda, Henry, Harry and Herman Harder for help, lodgings, beer and access  
594 to their land. Marvin Lamb, Ed Knott, Mike Holliday, Charmaine Despain, and Dave and John  
595 Schlomer are thanked for generous and unrestricted access to private land. Reviews by X and X.  
596 Jw/dg/Sr/Ph.

597

## 598 **References**

599 Aramaki, S., Hayakawa, Y., Fujii, T., Nakamura, K., Fukuoka, T., 1986. The October 1983 eruption  
600 of Miyakejima volcano. *J. Volcanol. Geotherm. Res.* 29, 203-229.

601

- Bretz, J.H., Smith, H.T.U., Neff, G.U., 1956. Channelled scabland of Washington—new data and interpretations. *Geol. Soc. Am. Bull.*, 67, 957-1049.
- Camp, V.E., Ross, M.E., 2004. Mantle dynamics and genesis of mafic magmatism in the intermontane Pacific Northwest. *J. Geophys. Res.*, 109, B08204. doi:10-1029/2003JB002838.
- Camp, V.E., Ross, M.E., Hanson, W.E., 2003. Genesis of flood basalts and Basin and Range volcanic rocks from the Steens Mountain to the Malheur River Gorge, Oregon. *Geol. Soc. Am. Bull.* 115, 105–128.
- Costantini, L., Bonadonna, C., Houghton, B.F., Wehrmann, H., 2009. New physical characterisation of the Fontana Lapilli basaltic Plinian eruption, Nicaragua. *Bull. Volcanol.* 71, 337-355.
- Costantini, L., Pioli, L., Bonadonna, C., Clavero, J., Longchamp, C., 2011. A Late Holocene explosive mafic eruption of Villarica volcano, Southern Andes: the Chamilla deposit. *J. Volcanol. Geotherm. Res.* 200, 143-158.
- Courtillot, V. Renne, P., 2003. On the ages of flood basalt events, *Comptus Rendus Geosci.* 335, 113-140.
- Head, J.W., Wilson, L., 1989. Basaltic pyroclastic eruptions: influence of gas release patterns and volume fluxes on fountain structure, and the formation of cinder cones, spatter cones, rootless flows, lava ponds and lava flows. *J. Volcanol. Geotherm. Res.*, 37, 261-271.
- Heliker, C., Kauahikaua J., Sherrod, D.R., Lisowski, M., Cervelli, P., 2003. The rise and fall of Pu‘u ‘Ō‘ō Cone, 1983-2002. In: Heliker, C., Swanson, D.A., Takahashi, T.J., (Eds). *The Pu‘u ‘Ō‘ō - Kūpāinaha eruption Kīlauea volcano, Hawai‘i: the first 20 years*. USGS Prof. Paper 1676, 29-52,
- Hon, K., Kauahikaua, J., Denlinger R., Mackay, K., 1994. Emplacement and inflation of pāhoehoe sheet flows: observations and measurements of active lava flows on Kilauea Volcano, Hawaii. *Geol. Soc. Am. Bull.*, 106, 351-370.
- Hooper, P.R., and Conrey, R.M., 1989. A model for the tectonic setting of the Columbia River basalt eruptions. In: Reidel, S.P., and Hooper, P.R., eds., *Volcanism and tectonism in the Columbia River flood basalt province*: *Geol. Soc. Am. Spec. Paper*, 239, 293-306.
- Houghton, B. F., Wilson, C.J.N., 1989. A vesicularity index for pyroclastic deposits. *Bull. Volcanol.*, 51, 451-462
- Houghton, B.F., Wilson, C.J.N., Fierstein, J., Hildreth, W., 2004. Complex proximal deposition during the Plinian eruptions of 1912 at Novarupta, Alaska. *Bull. Volcanol.* 66, 95-133.
- Houghton, B.F., Gonnermann, H.M., 2008. Basaltic explosive volcanism: constraints from deposits and models. *Chemie der Erde*, 68, 117-140.
- Lund, K., and Snee, L.W., 1988. Structural development and age of the continent-island arc juncture in west-central Idaho: in Ernst, W.G., (Ed) *Metamorphism and crustal evolution of the western United States*, Prentice-Hall, Englewood Cliffs, 296-331.

- Mannen K., Ito, T., 2007. Formation of scoria cone during explosive eruption at Izu-Oshima volcano, Japan. *Geophys. Res. Lett.*, 34, L18302, ODI:10.1029/2007GL030874.
- Martin, B.S., 1989. The Roza Member, Columbia River Basalt Group: Chemical stratigraphy and flow distribution. In: Reidel, S.P., and Hooper, P.R., eds., *Volcanism and tectonism in the Columbia River flood basalt province*: Geol. Soc. Am. Spec. Paper, 239, 85–104.
- Olsen, P.E., 1999. Giant lava flows, mass extinctions, and mantle plumes, *Science*, 293, 604-605.
- Parcheta, C.E., Houghton, B.F., Swanson, D.A., 2012. Hawaiian fissure fountains 1: decoding deposits—episode 1 of the 1969-1974 Mauna Ulu eruption. *Bull. Volcanol.* DOI: 10.1007/s00445-012-0621-1.
- Porter, S.C., 1972. Distribution, Morphology, and size frequency of cinder cones on Mauna Kea volcano, Hawai‘i. *Geol. Soc. Am. Bull.*, 83, 3607-3612.
- Pyle, D.M., 1989. The thickness, volume and grainsize of tephra fall deposits. *Bull Volcanol.* 51, 1-15.
- Rampino M.R., Stothers R.B., 1988. Flood basalt volcanism during the past 250 million years. *Science*, 241, 663-668.
- Reidel, S.P., 1984. The Saddle Mountains—the evolution of an anticline in the Yakima fold belt. *American Journal of Science*, 284, 942-978.
- Reidel, S.P., & Tolan, T.L. 1992. Eruption and emplacement of flood basalt: An example from the large- volume Teepee Butte Member, Columbia River Basalt Group. *Geol. Soc. Am. Bull.*, 104, 1650-1671.
- Ross, P.-S. Ukstins Peate T, I., McClintock M.K., Xu, Y.G. Skilling, I.P. White, J.D.L. Houghton B.F., 2005. Mafic volcanoclastic deposits in flood basalt provinces: A review. *J. Volcanol. Geotherm. Res.*, 145, 281– 314
- Sable, J.E., Houghton, B.F., Wilson, C.J.N., Carey, R.J., 2006. Complex proximal sedimentation from Plinian plumes: the example of Tarawera 1886. *Bull. Volcanol.* 69, 89-103
- Saunders, A., Reichow, M. 2009. The Siberian Traps and the end-Permian extinction: a critical review. *Chin. Sci. Bull.* 54, 20-37.
- Sparks, R.S.J., Wright, J.V., 1979. Welded air fall tuff. In: Chapin CE, Elston WE (Eds), *Ash flow tuffs*. Spec. Paper Geol. Soc. Am., 180, 155-166.
- Sparks R.S.J. Bursik M.I., Carey. S.N., Gilbert, J.S., Glaze, L.S., Sigurdsson, H., Woods, A.W., 1997. *Volcanic plumes*. Wiley, pp. 590.
- Stothers, R.B., Wolff, J.A., Self, S., Rampino, M.R., 1986. Basaltic fissure eruptions, plume heights, and atmospheric aerosols. *Geophys. Res. Lett.* 13, 725-728.
- Sumner, J.M., 1998. Formation of clastogenic lava flows during fissure eruption and scoria cone collapse: the 1986 eruption of Izu-Oshima volcano, eastern Japan. *Bull. Volcanol.* 60, 195-212.

- Sumner, J.M. Blake S., Matela R.J., Wolff J.A., 2005. Spatter. *J. Volcanol. Geotherm. Res.* 142, 49-65.
- Swanson, D.A., Wright, T.L., and Helz, R.T., 1975. Linear vent systems and estimated rates of magma production and eruption for the Yakima basalt of the Columbia plateau. *American Journal of Science*, 275, 877-905.
- Thomas, R.M.E., Sparks, R.S.J., 1992. Cooling of tephra during fallout from eruption columns. *Bull. Volcanol.* 54, 542-553.
- Thordarson, T., 1991. The 1783–84 Laki eruption: Tephra production and course of events. University of Iceland Special Publication, F90018. University of Iceland Press, Reykjavik, 187p.
- Thordarson, T., Self, S., 1993. The Laki (Skaftár Fires) and Grímsvötn eruptions in 1783–1785. *Bull. Volcanol.* 55, 233–263.
- Thordarson, T., Self, S., 1996. Sulfur, chlorine and fluorine degassing and atmospheric loading by the Roza eruption, Columbia River Basalt Group, Washington, USA. *J. Volcanol. Geotherm. Res.*, 74, 49-73.
- Thordarson, T., and Self, S., 1998. The Roza Member, Columbia River Basalt Group: a gigantic pahoehoe lava flow field formed by endogenous processes. *Journal of Geophysical Research*, 103, 27,411-27,445.
- Thordarson, T., Miller, D.J., Larsen, G., Self, S., Sigurdsson, H., 2001. New estimates of sulfur degassing and atmospheric mass-loading by the 934 Eldgjá eruption, Iceland. *J. Volcanol. Geotherm. Res.*, 108, 33-54.
- Thordarson, T., Rampino, M., Keszthelyi, L.P., Self, S., 2009. Effects of megascale eruptions on Earth and Mars. In: Chapman, M.G., Keszthelyi, L.P., eds, *Preservation of random megascale events on Earth and Mars: influence on geologic history*. *Geol. Soc. Am. Spec. Paper*, 453, 37-53.
- Tolan, T.L., Beeson, M.H., Anderson, J.L., Fecht, K.R., and Swanson, D.A., 1989. Revisions to the estimates of the areal extent and volume of the Columbia River Basalt Group. *Geol. Soc. Am. Spec. Paper*, 239, 1-20.
- Tolan, T.L., Martin, B.S., Reidel, S.P., Kauffman, J.D., Garwood, D.L., and Anderson, J.L., 2009. An introduction to the stratigraphy, structural geology and hydrogeology of the Columbia River Flood-basalt Province: a primer for the GSA Columbia River Basalt Group field trips. In: O’Conner, J., (Ed) *Volcanoes to vineyards: geologic field trips through the dynamic landscape of the Pacific Northwest*, GSA Field Guides, 15, 599-643.
- Vergnolle, S., Caplan-Auerbach, J., 2006. Basaltic thermals and Subplinian plumes: constraints from acoustic measurements at Shishaldin volcano, Alaska. *Bull. Volcanol.* 68, 611-630.
- Walker, G.P.L., Self, S., Wilson, L., 1984. Tarawera 1886, New Zealand—a basaltic Plinian fissure eruption. *J. Vo.* 60, 432-440.

750 Wolfe, E.W., Neal, C.A., Banks, N.G., Duggan, T.J., 1988. The Puu Oo eruption of Kilauea volcano,  
 751 Hawai'i: episodes 1 through 20, January 3, 1983, through June 8, 1984. US Geol. Surv. Prof. Paper  
 752 1463.  
 753  
 754 Wolff, J.A., Ramos, F.C., Hart, G.L., Patterson, J.D., and Brandon, A.D., 2008. Columbia River  
 755 flood basalts from a centralized crustal magmatic system. *Nature Geosci.* 1, 177-180.  
 756  
 757 Wolff, J.A., Sumner, J.M., 2000. Lava fountains and their products. In: Sigurdsson, H., Houghton  
 758 B.F., McNutt, S.R., Rymer, H., Stix, J., *Encyclopedia of Volcanoes*, Academic Press, San Diego,  
 759 321-330.  
 760  
 761 Wood, C.A., 1980. Morphometric evolution of cinder cones. *J. Volcanol. Geotherm. Res.* 7, 387–  
 762 413.  
 763  
 764 Woods, A.W., 1993. A model of the plumes above basaltic fissure eruptions. *Geophys. Res. Lett.* 20,  
 765 1115-1118.  
 766

767 **Figure Captions**

768 **Figure 1.** A. Sketch map of the Columbia River Basalt Province (grey shaded), showing the extent  
 769 of the Roza Member (solid white line) and the Roza vent system (black solid line). WISZ – Western  
 770 Idaho Shear Zone marks the location of the continental suture. Large grey oval is the inferred  
 771 position of the CRBP basaltic magma storage zones/source region according to Wolff et al. (2008).  
 772 Dotted ovals are dikes swarms: M – monument dike swarm; CJ Chief Joseph dike swarm. B. Map of  
 773 the northern end of the Roza vent system (area enclosed in rectangle on A) showing outcrops of  
 774 pyroclastic rocks and names of recognized vent accumulations.

775  
 776 **Figure 2.** Pyroclastic lithofacies of the Roza Member (see also Table 1 and Fig. 1 for locations). A)  
 777 Non-welded scoria fall deposit (ScL, Winona). B) Weakly agglutinated scoria lapilli (waScL, Rock  
 778 Creek Center). C) Moderately agglutinated scoria lapilli (maScL) and spatter bombs (Sp; Buffalo  
 779 Spring South). Scale in centimeters. D) Densely agglutinated scoria (dwScL) with pronounced  
 780 columnar joints (Texas Draw). Base of unit is marked by arrows. E) Densely agglutinated spatter  
 781 (dwSpB; Texas Draw). F) Lava-like densely welded spatter with wispy streaky fiamme (llwSp,  
 782 Texas Draw). G) Clastogenic lava with heterogeneous patchy vesiculation (clLava, Texas Draw). H)

783 Pyroclastic lithic breccia composed of Roza lava overlain by non-welded scoria fall deposit (Rock  
784 Creek Center, see Fig. 1 and 6). Rule with 10 cm divisions.

785

786 **Figure 3.** Microtextural features of the Roza pyroclastic rocks seen in thin section. Site locations  
787 mentioned are shown on Fig. 1. A) Pristine scoria fall deposit from Winona (see also Fig 2A). Clast  
788 has a density of  $720 \text{ kg/m}^3$  corresponding to a vesicularity of  $\sim 75 \text{ vol. \%}$ . B) Achneliths (Pele's tears)  
789 in moderately agglutinated fall deposit at Rock Creek East (Fig 1). Note the moderate amount of  
790 welding compaction of clasts. C) Densely agglutinated spatter deposit (Texas Draw, see also Fig 2E).  
791 Note moderate, welding-induced, bedding-parallel alignment of plagioclase phenocrysts sitting in a  
792 microcrystalline groundmass.

793

794 **Figure 4.** Pyroclastic deposits of the Buffalo Spring North (BSN) and Buffalo Spring South (BSS)  
795 vent accumulations: A) Panorama looking east of Buffalo Spring south vent constructs, showing  
796 dipping beds and onlapping Roza sheet lobes. Cattle and telegraph pole for scale. B) Geological map  
797 of BSN vent deposits that form part of edifice with flanks dipping to NW, W and SW. C) Geological  
798 map of BSS vent deposits which form SW end of edifice with flanks dipping to SE, E and S. See key  
799 for details. Steep inward dipping beds are inferred to mark the position of the crater. D) Measured  
800 section through BSN showing lithological, density and clast flattening ratios with height  
801 (abbreviations are explained in Table 1).

802

803 **Figure 5.** Pyroclastic deposits of the Rock Creek vent accumulations. A) Panorama looking east of  
804 the Rock Creek Center (RCC) deposits, showing pyroclastic beds thinning southwards over early  
805 Roza lavas. B) Cross-section through the RCE edifice with interpretation for how it may have  
806 originally looked. C) Dipping beds of predominantly weakly and moderately agglutinated scoria  
807 (RCC). E) Geological map of Rock Creek showing the west, center and east vents.

808

809 **Figure 6.** Measured sections through the Rock Creek Center cone deposits (see also Fig. 5), showing  
810 variation with height in lithology, grainsize (solid black line), density (average and range of 10  
811 measurements) and clast aspect ratio (average of 10 measurements). Abbreviations for lithofacies are  
812 given in Table 1.

813

814 **Figure 7.** Pyroclastic deposits of the Texas Draw (TD) vent accumulations (see Fig. 1 for location of  
815 site). A) Photo-interpretation of the pyroclastic edifice at TD, looking west. B) Geological map of  
816 Texas Draw (see Fig. 4 for key). Note rapidly changing dips and strikes in the southern half of map.  
817 C) Composite section through the southern half of the pyroclastic edifice (see A) showing vertical  
818 changes in lithology, density, clast aspect ratio and grainsize. D) Bedded sequence of weakly to  
819 densely agglutinated scoria on west side of TD. Ruler for scale, divisions = 10 cm. E) dipping strata  
820 at northern end of TD edifice. Horizontal sheet lobes in the distance onlap against the edifice. For  
821 key see Fig. 4.

822

823 **Figure 8.** Pyroclastic deposits at the Winona vent (see Fig. 1 for location of site). A) Geological map  
824 of the pyroclastic deposits immediately south and east of Winona (see Fig. 4 for key) X-Y-Z is line  
825 of section in B; X also marks location of Winona village. B) Scaled cross-section ( $4 \times$  vertical  
826 exaggeration) through the Winona vent accumulations. Note the opposing flanks of densely  
827 agglutinated spatter terminating abruptly at the inferred vent. C) Eastern spatter mound with fiamme  
828 (arrows) dipping gently to the east. For key see Fig. 4.

829

830 **Figure 9.** A) Histogram of dip magnitudes of bedding planes and welding fabrics in pyroclastic  
831 deposits around Roza vents. B) Plot of flattening ratio against mean density (average of 10  
832 measurements) for pyroclastic deposits of the Roza Member. C) Histogram of the densities of 16–32

833 mm scoria lapilli from a scoria fall deposit 1.7 km from vent at Winona (n=100). D) Grainsize  
834 distribution of the Roza fall deposit in C compared to similar deposits from historical eruptions. The  
835 Laki and Eldgja samples were collected from sites <1.5 km from the vents and are representative for  
836 the fall deposit in the proximal/near vent region (Thordarson, 1991).

837

838 **Figure 10.** Cartoon illustrating a sustained convective column developed above a vent in the Roza  
839 eruption. Fallout from tall fountains supplemented by fallout from the margins of the lower parts of  
840 convective columns result in high aggradation rates ( $>> 20$  cm/min) and the construction of broad  
841 wide agglutinate cones dominated by welded and agglutinated deposits.

842

843

844

845

846

847

848

849

850

851

852

853

854

855

856

857

858

859

860

861

862

863

864

865

866

867

868

869

870

871

872

873



lithofacies	$\rho$ (kg m <sup>-3</sup> )	clast aspect ratio	description	interpretation
scoria lapilli (ScL)	300– 1100	N/A	<b>Composition:</b> well-sorted, clast-supported, black, angular moderately to highly vesicular scoria lapilli, bombs and coarse ash; variably altered; clasts exhibit fractured surfaces, fluidal exteriors; achneliths common; <b>Structure:</b> massive; rare thin beds defined by slight grainsize variation; occurs in units up to 3 m thick. <b>Occurrence:</b> medial fall deposit > 300 m from inferred vents; interbedded with other pyroclastic lithofacies in proximal regions and in between pahoe-hoe lobes at distances > 500 m from source; coarsens towards source.	Fall deposit from sustained eruption plume above Hawai'ian fire fountain.
weakly agglutinated scoria lapilli (waScL)	1200– 1400	1:1–1:3	<b>Composition:</b> As ScL; clasts stuck together at point contacts; <b>Structure:</b> massive; small amounts of clast deformation; minor reduction in deposit pore space; occurs in units up to 1 m thick. <b>Occurrence:</b> as ScL; proximal and medial deposit.	As above; higher accumulation rates promoted agglutination at point contacts
moderately agglutinated scoria lapilli (maScL)	1200– 1800	1:1.3–1:6	<b>Composition:</b> moderately well sorted clast-supported scoria lapilli and bombs up to 15 cm in diameter; black to orange (oxidised in color); commonly glass of clasts has been altered to clay. Achneliths common. <b>Structure:</b> individual clast outlines visible; moderate deformation of clasts; massive to crudely bedded; bedding defined by grainsize; occurs in units from 0.5–14 m thick <b>Occurrence:</b> proximal cone-building deposits and sheet-forming deposits; interbedded with other proximal lithofacies.	Fallout from lava fountain; elevated accumulation rates promoted agglutination.
densely welded scoria lapilli (dwScL)	1500– 2200	1:2–1:15	<b>Composition:</b> as wScL; clasts up to up to 15 cm; clast outlines poorly visible; variable vesicularity. <b>Structure:</b> massive; in beds up to 3 m thick; strong eutaxitic texture; characterised by poor to well developed columnar joints; complete loss of deposit pore space. <b>Occurrence:</b> proximal cone-building deposits and sheet-forming deposits.	Fallout from inner parts of lava fountain; rapid accumulation rates promoted dense agglutination and allow cooling joints to form.
densely welded spatter (dwSp)	1700– 2800	1:3–1:20	<b>Composition:</b> densely welded spatter bombs up to 90 cm. <b>Structure:</b> massive; sharp contacts; intense clast deformation with high aspect ratio fiamme; complete loss of pore space; occurs in units from 0.5–10 m thick; <b>Occurrence:</b> proximal cone-building deposits.	Fallout of large spatter clasts under inner parts of lava fountain.
lava-like densely welded spatter (llwSp)	2200– 2700	N/A	<b>Composition:</b> vitrophyric non-vesicular glass; clast outlines not visible; rare wispy vesicular fiamme present in some outcrops; <b>Structure:</b> massive; cm-spaced platy joints or poorly developed columnar joints; hackly fracture; occurs in units 2.5–>5 m thick; absence of chilled margins. <b>Occurrence:</b> proximal cone-building deposits.	Fallout of fluidal spatter clasts from inner fountain; rapid accumulation rates; clasts coalesce on deposition
clastogenic lava (clLava)	1600– 2000	N/A	<b>Composition:</b> crystalline lava with irregular distribution of vesicles; outlines of clasts defined by vesicle patches. <b>Structure:</b> massive; forms units up to 0.3–2 m thick. <b>Occurrence:</b> cone-building deposits and sheet-forming deposits; interbedded with proximal pyroclastic lithofacies.	Coalescence of pyroclasts at base of fountain; flows away as lava.
Breccia (Br)	>2700	N/A	<b>Composition:</b> clast-supported angular blocks of lava. <b>Structure:</b> massive; poorly exposed <b>Occurrence:</b> proximal edifice at Rock Creek Centre vent.	Formed by explosive eruptions; ballistically-emplaced clasts

887 **Table 1.** Summary description and interpretation for pyroclastic lithofacies of the Roza Member.  
888

pyroclastic vent	Location (Deg. Min. Sec)	description
Harder Ranch	47° 4'47.44"N 118° 0'33.80"W	Dipping beds (0–32°) of densely agglutinated scoria and spatter poorly exposed over 0.27 km <sup>2</sup> ; bedding defines a partial cone with dips to the N, W and SW, an apparent radius of >350 m and length of >500 m; oldest deposits are lava-like densely welded spatter; spatter bombs > 50 cm in diameter; base of pyroclastic deposits not seen; overlapped by Roza sheet lobes and Rosalia Member.
Rock Creek North	47° 2'39.51"N 117°57'9.64"W	Bedded moderately to densely agglutinated scoria and spatter outcropping over 0.1 km <sup>2</sup> ; Bedding dips (3–31°) define a half-cone with slopes to the NW, N and NE, a radius of ~250 m and a length of 450 m; ropey-surfaced vesicular spatter bombs reach 45 cm in diameter; overlapped by Roza sheet lobes.
Rock Creek West	47° 1'2.01"N 117°57'2.31"W	4 m of lava-like densely welded spatter passing up into 5 m of bedded weakly and moderately agglutinated scoria; dense spatter bombs up to 6 m in diameter; vesicular spatter bombs up to 80 cm in diameter; Beds dip north and west and may define a partial cone or drape underlying lava topography; overlies Roza sheet lobe (as Rock Creek Center).
Palouse River	46°55'13.10"N 117°50'48.42"W	Flat-lying beds of moderately to densely agglutinated spatter and lava-like spatter exposed in bluffs along Palouse River; rafted spatter ramparts overlie capping Roza sheet lobe.
*Union Flat Creek	46°52'9.84"N 117°45'57.34"W	Small roadcut exposing >2 m of densely agglutinated spatter overlying Roza sheet lobe; thin scoria fall deposit exposed in road cuts to east with welded top.
*Megginson Gulch	46°26'35.71"N 117°24'19.50"W	Discontinuous road cuts through densely welded and agglutinated spatter and spongy pāhoehoe lobes.
*Potter White Hill [15]	46°19'15.00"N 117°21'8.81"W	Road cut and small quarry in moderately to densely welded spatter and chaotic agglutinate meso-breccias; interpreted as crater deposits (Brown et al., in press).
*Little Butte [16]	46° 8'29.92"N 117°16'20.41"W	Poorly exposed densely welded spatter and dense lava interpreted as lava shield volcano (Swanson et al., 1975)
*Big Butte [17]	46° 6'52.25"N 117°15'10.94"W	As Little Butte.
Crow Creek	45°37'28.37"N 117° 8'23.14"W	Road cuts and borrow pit through steeply dipping non-welded fall deposits, moderately to densely agglutinated scoria and spatter, spongy pāhoehoe, clastogenic lava and breccia; deposits occur within conduit cut through Grande Ronde lavas; interpreted as conduit deposits.

889  
890  
891 **Table 2.** Summary information for poorly exposed vents and pyroclastic deposits of the Roza  
892 Member not described in the text and arranged from north to south. \*localities of Swanson et al.,  
893 (1975); numbers in square brackets are their numbering scheme. For location see Figure 1C.  
894  
895  
896  
897  
898  
899  
900  
901  
902  
903  
904  
905  
906  
907  
908  
909  
910  
911  
912  
913  
914  
915  
916  
917

918

Vent	Location	<sup>1</sup> masl	<sup>2</sup> trend	<sup>3</sup> l (km)	<sup>4</sup> r (km)	<sup>5</sup> area (km <sup>2</sup> )	$\theta_{\text{min-max}}$	$\theta_x$	$\theta_{\sigma}$	<sup>6</sup> h <sub>min</sub> (m)	<sup>7</sup> h <sub>max</sub> (m)
Harder Ranch	47° 4'50.28"N 118° 0'32.17"W	513	NNE-SSW	0.5	0.35	0.27	2–32°	17°	8°	53	107
Buffalo Spring (N)	47° 4'15.20"N 117°59'46.17"W	495	N-S	0.56	0.33	0.29	6–35°	15°	6°	51	88
Buffalo Spring (S)	47° 3'49.75"N 117°59'7.17"W	485	N-S	0.28	0.2	0.08	6–31°	16°	8°	50	57
Rock Creek (N)	47° 2'35.65"N 117°57'11.64"W	495	NNE-SSW	0.43	0.25	0.17	3–31°	19°	8°	46	86
Rock Creek (C)	47° 1'13.37"N 117°56'41.91"W	460	NNW-SSE	0.5	0.22	0.17	*12–24°	-	-	30	63
Rock Creek (E)	47° 1'26.86"N 117°56'6.48"W	480	NNE-SSW	0.41	0.23	0.15	13–44°	19°	9°	40	79
Texas Draw	46°58'47.63"N 117°52'55.02"W	480	N-S	0.56	0.22	0.19	6–37°	16°	8°	35	63
Mason Draw	46°57'4.11"N 117°51'3.91"W	470	NNE-SSW	0.9	0.5	0.71	9–27°	18°	7°	25	162
Winona	46°56'26.34"N 117°48'47.97"W	450	-	-	0.42	-	5–9°	-	-	15	15

919

920

921

922

923

924

925

926

927

928

929

930

931

932

933

934

935

936

937

938

939

940

941

942

943

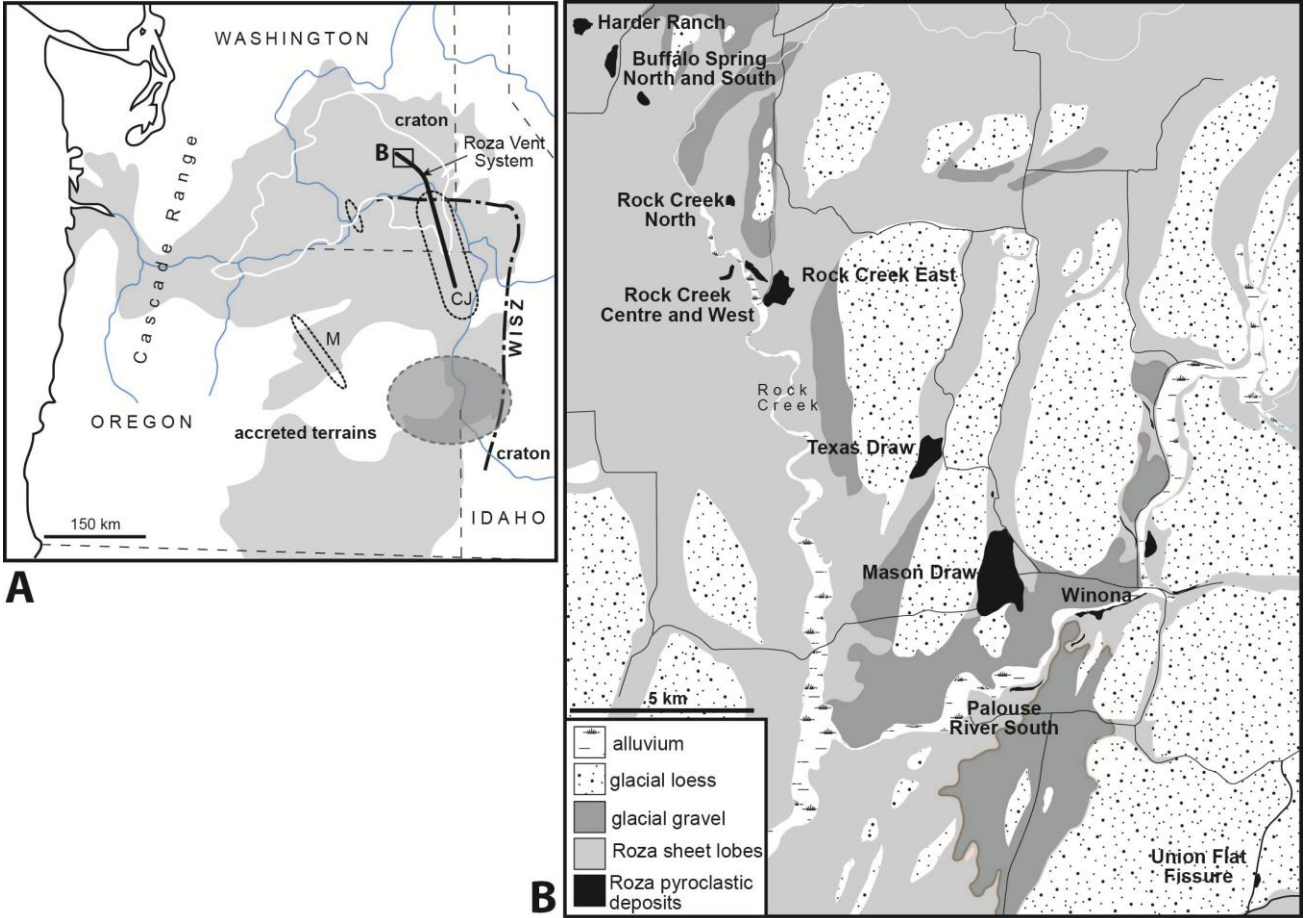
944

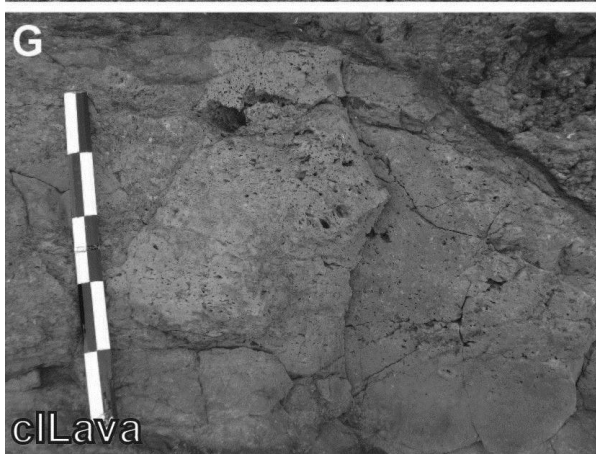
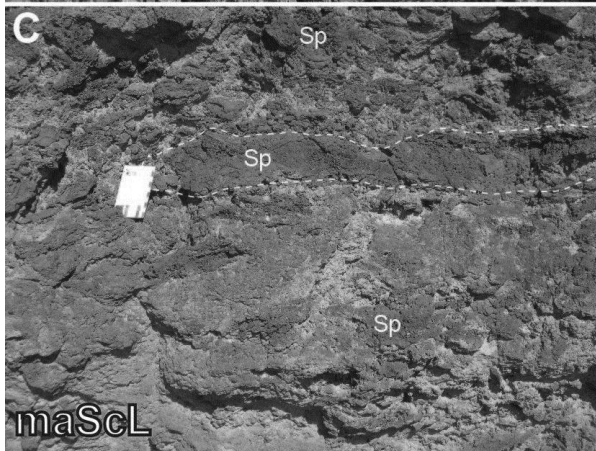
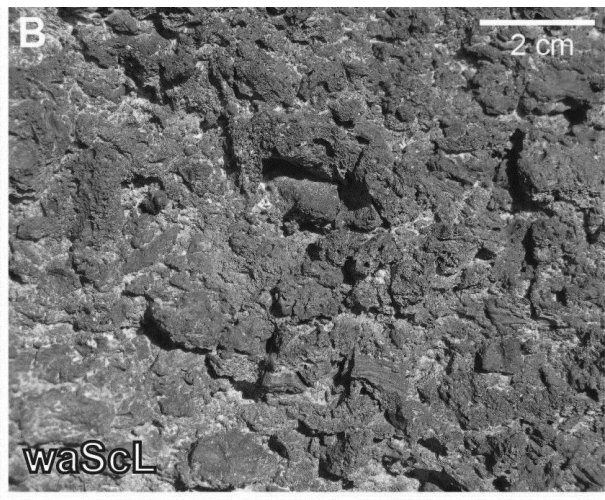
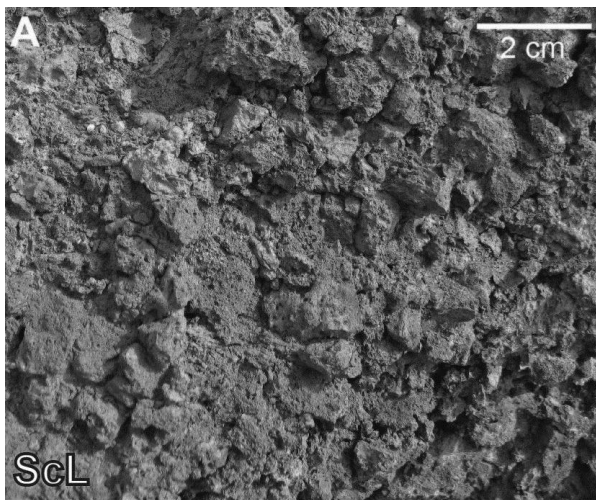
945

946

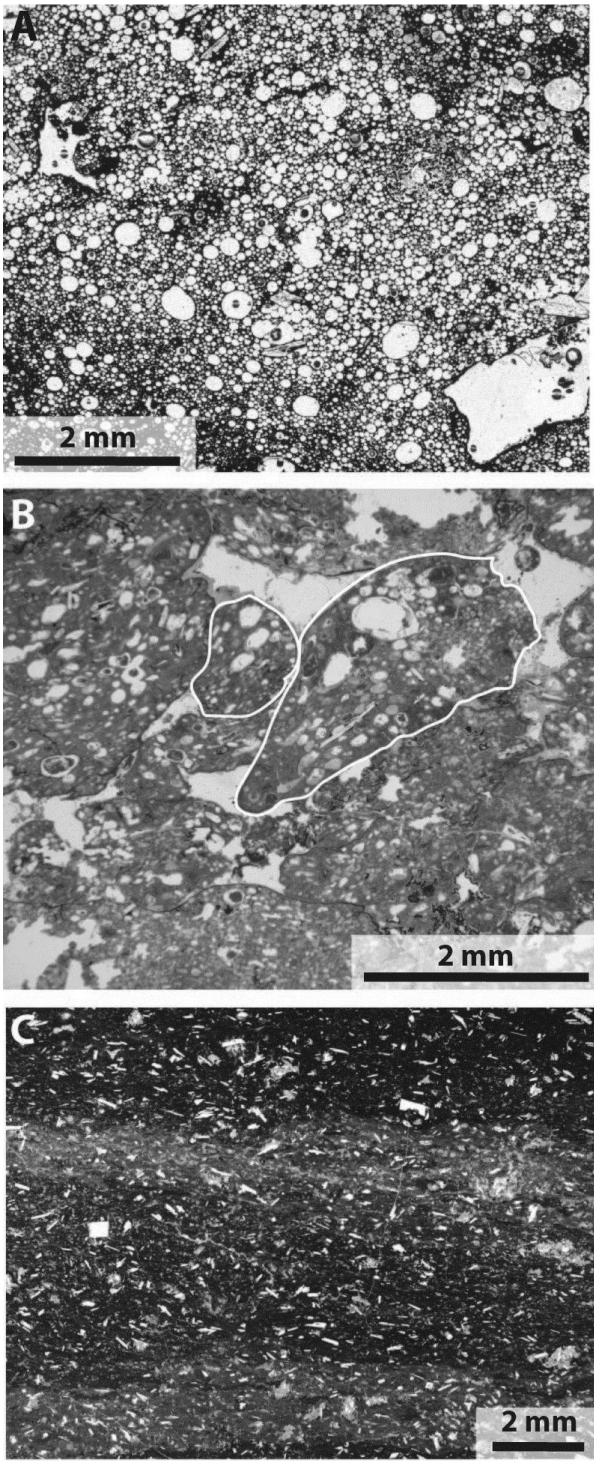
947

**Table 3.** Dimensions of pyroclastic cone remnants at vent localities. Orientation of cones estimated from bedding and foliation dips. <sup>1</sup>altitude of lowest exposed pyroclastic bed; <sup>2</sup>parallel to elongation of cone structure; <sup>3</sup>length parallel to cone structure/trend of fissure; <sup>4</sup>radius - orthogonal radius; <sup>5</sup>equivalent ellipse ( $a = 0.5 \pi r l$ ) <sup>6</sup>minimum height of cone using 460 m altitude as datum (base of pyroclastic successions at Winona and Rock Creek); <sup>7</sup>reconstructed by projecting average welding foliation dips ( $\theta_x$ ). \*limited data; dip of 16° used to calculate h<sub>max</sub>.



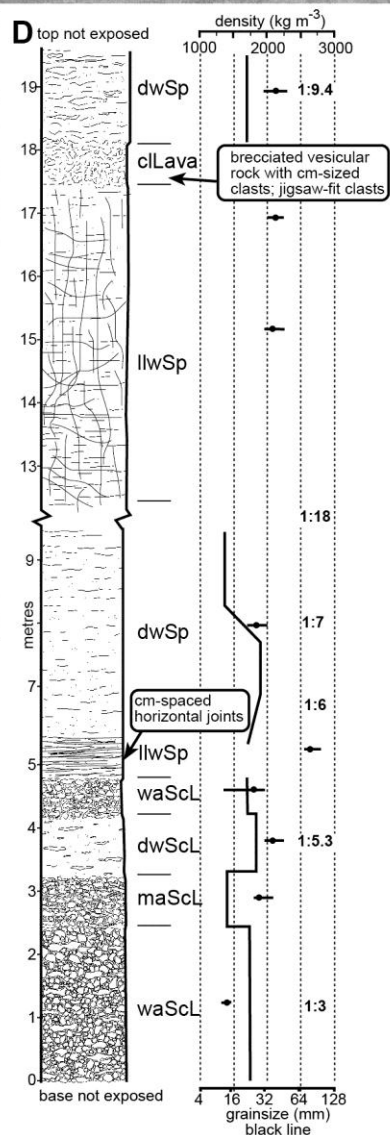
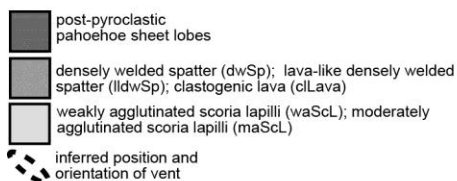
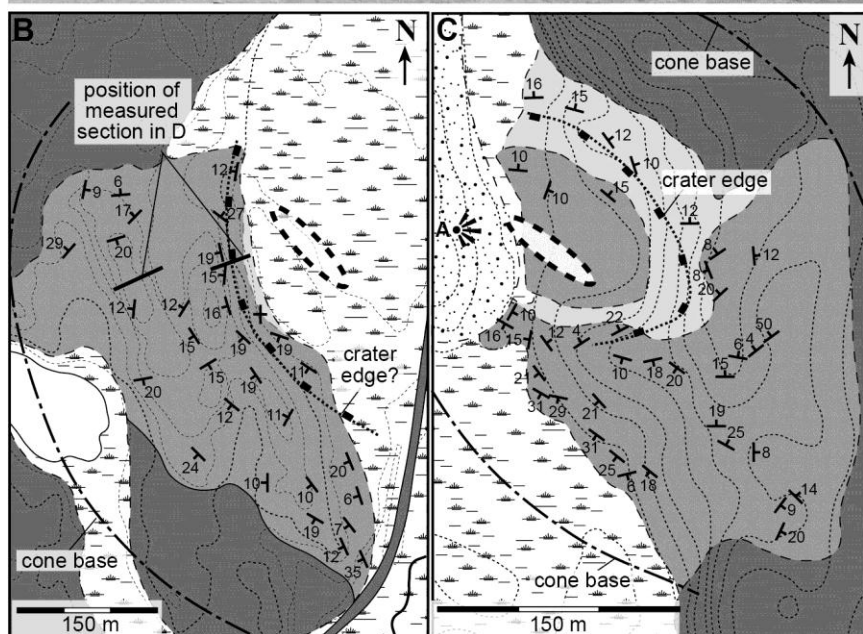


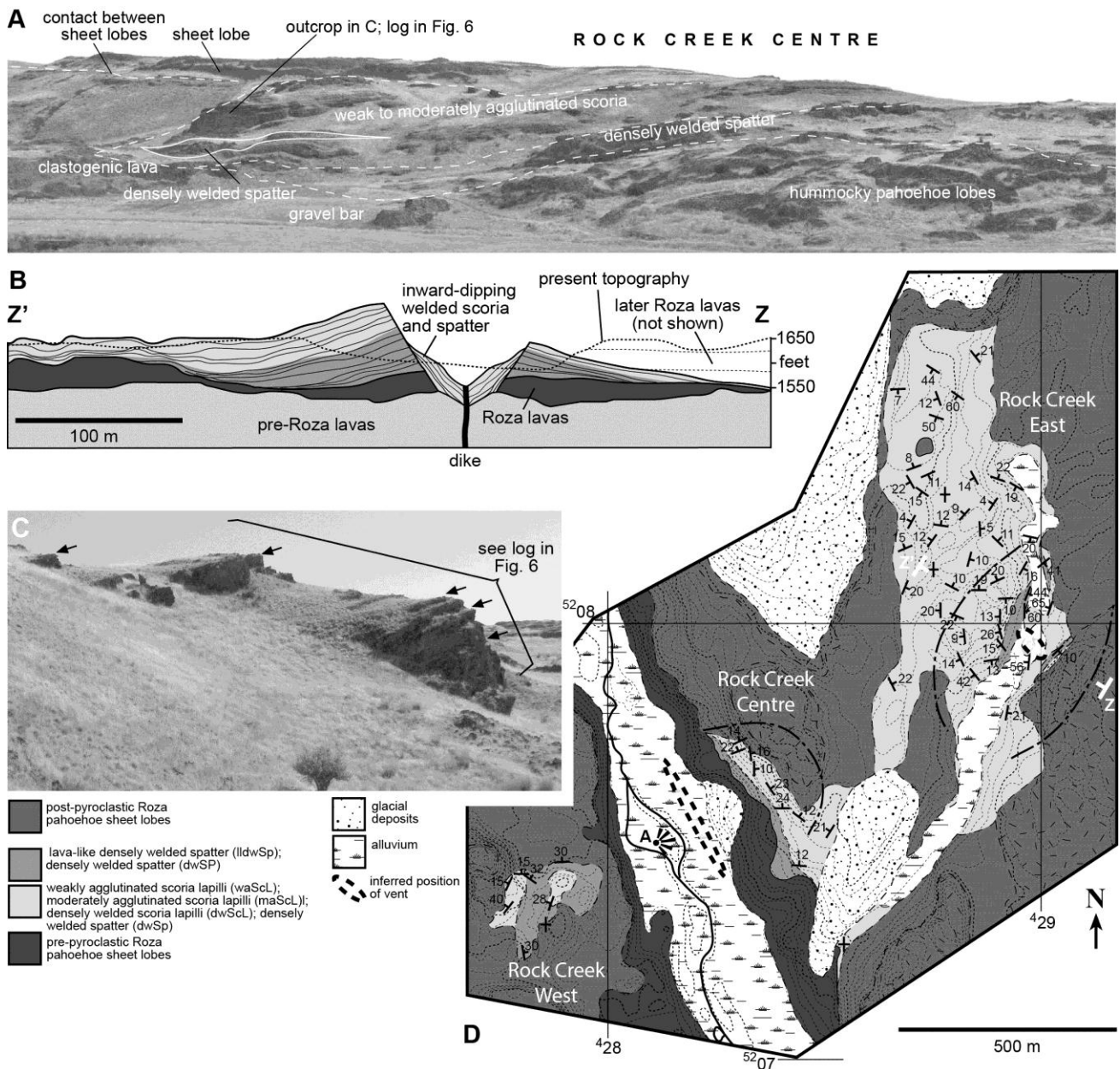
965



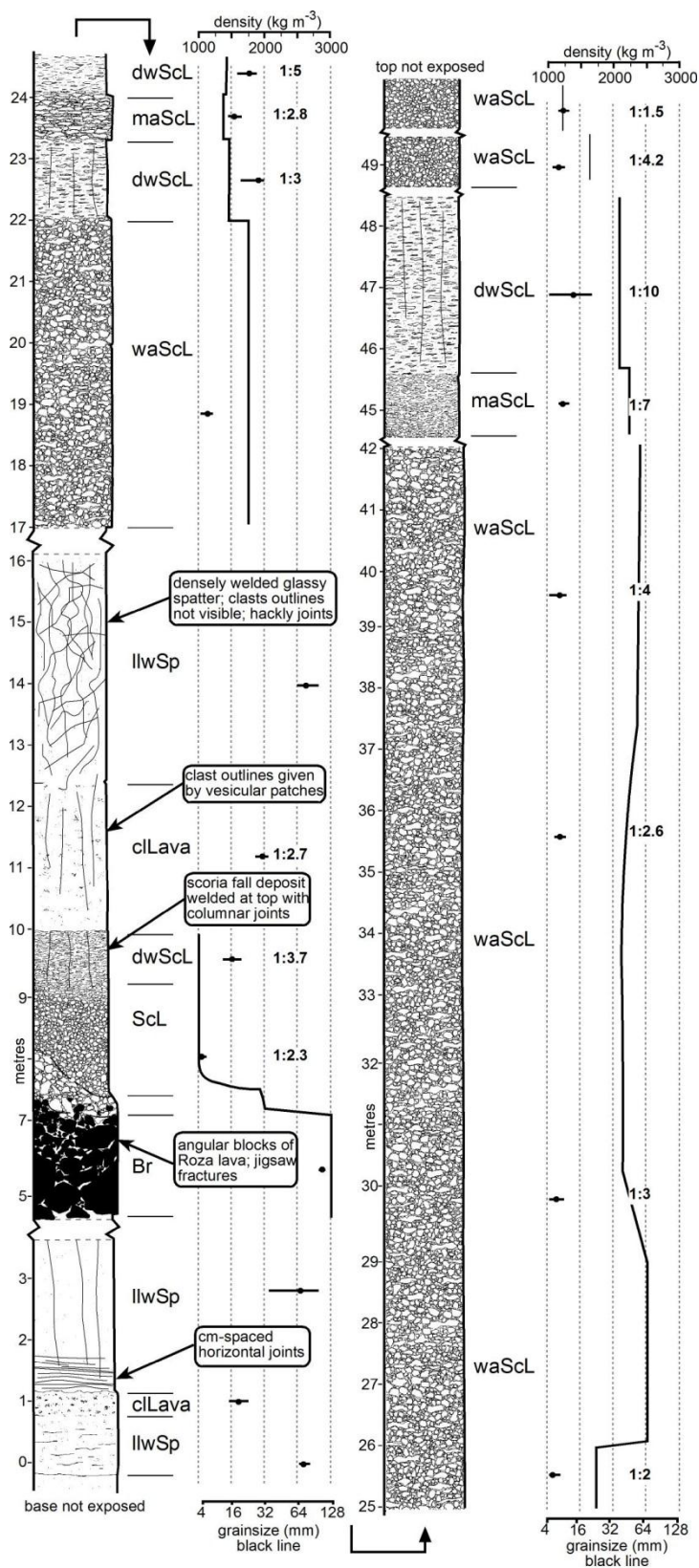
966  
967  
968  
969  
970  
971  
972



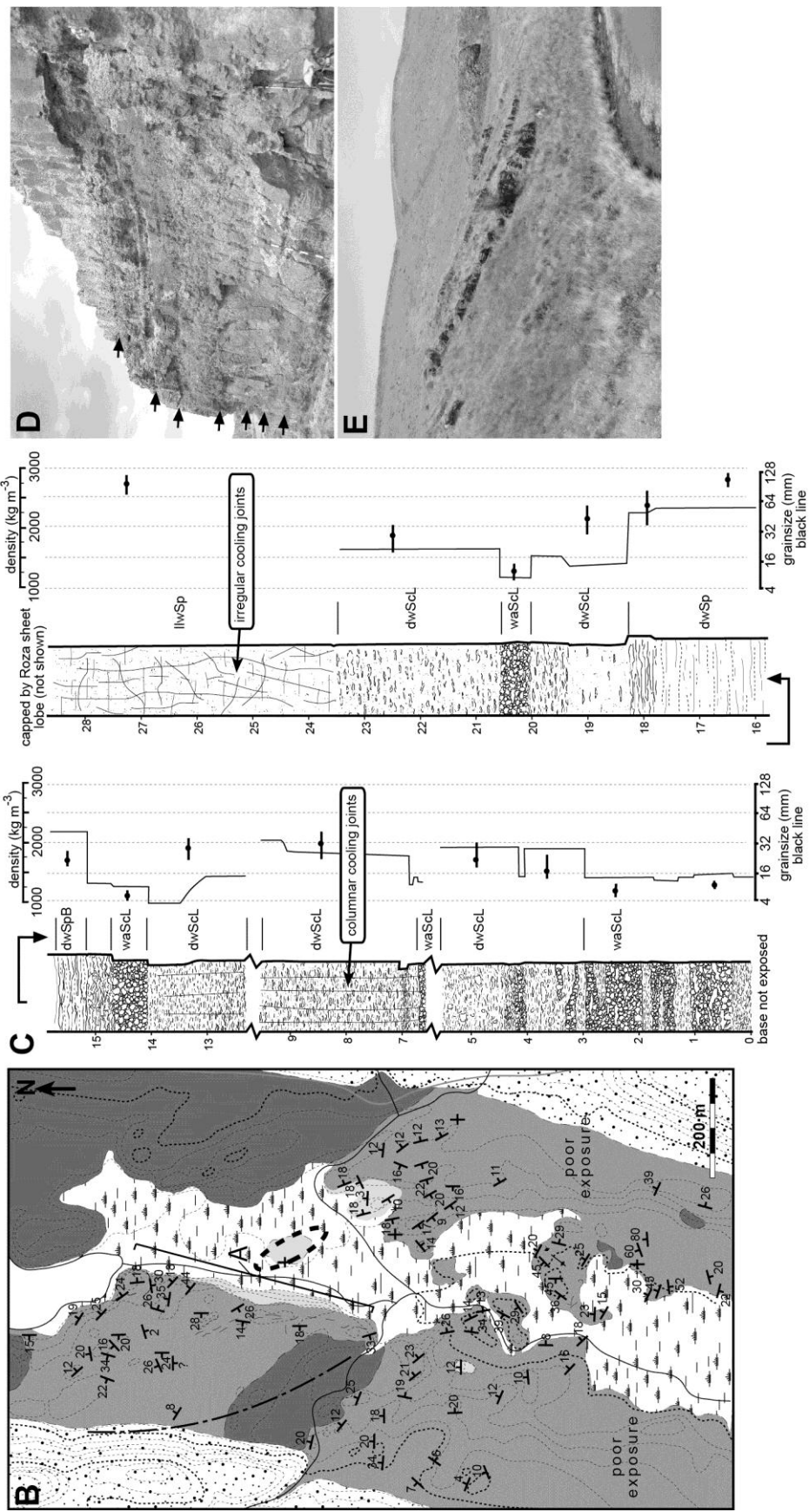
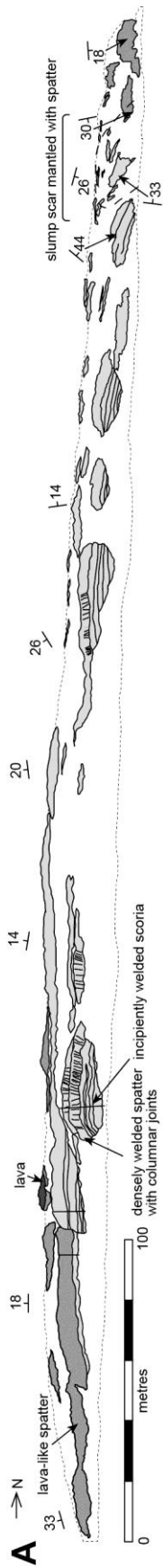


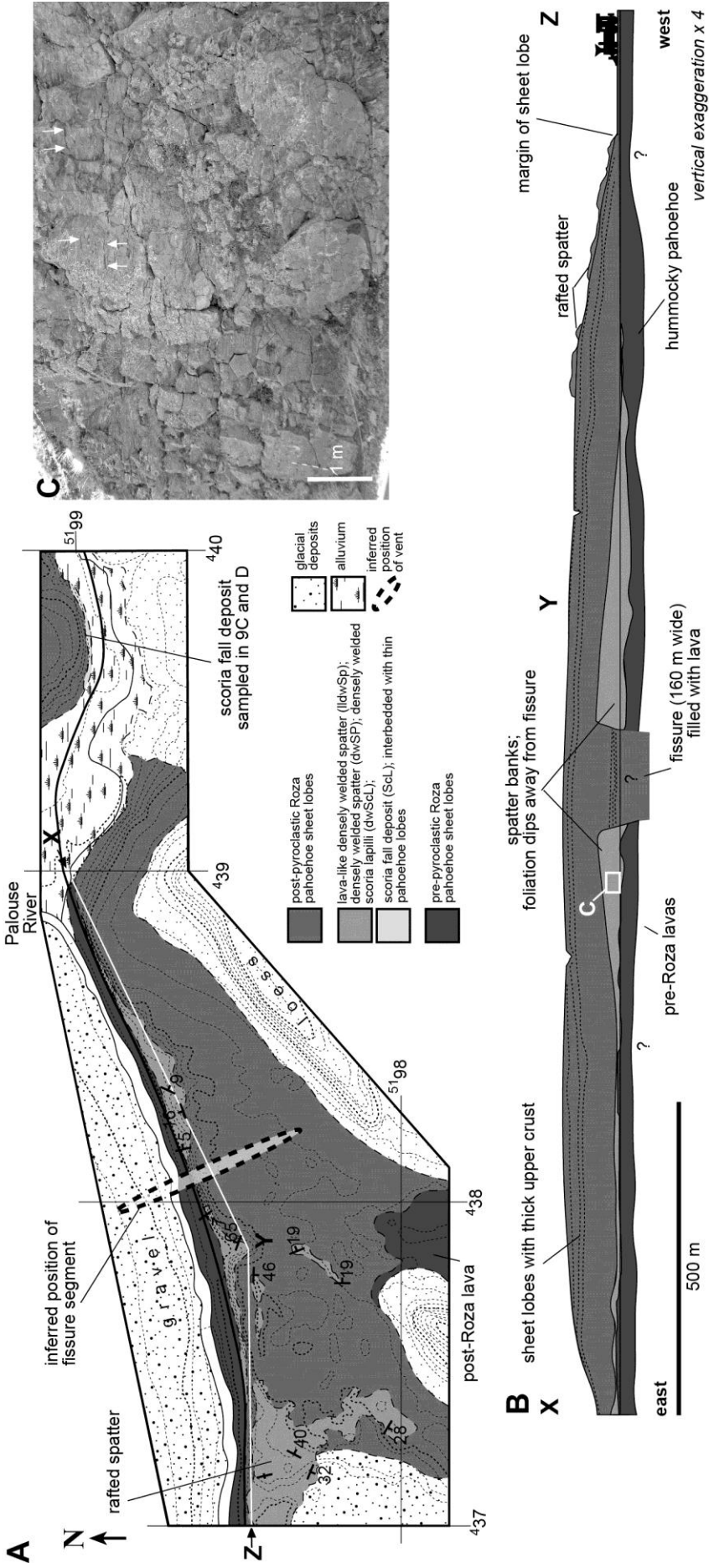




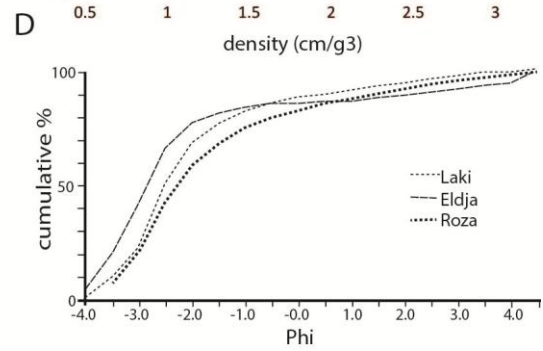
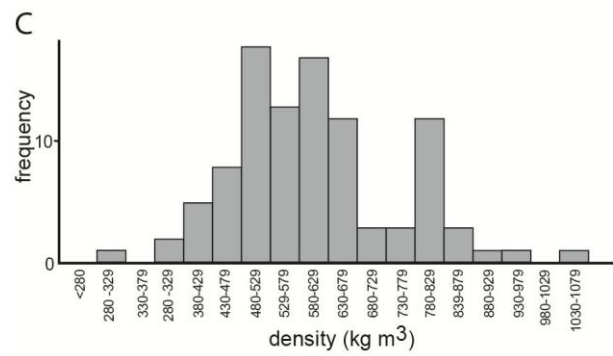
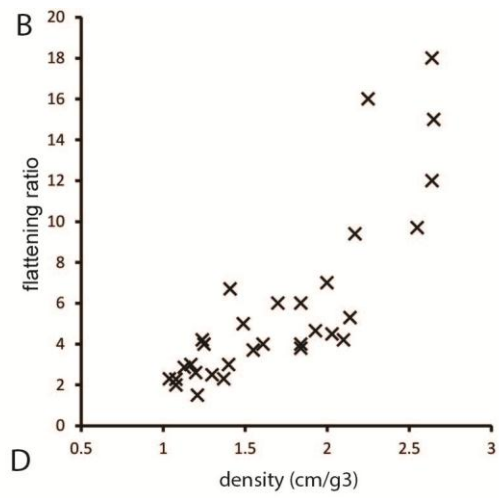
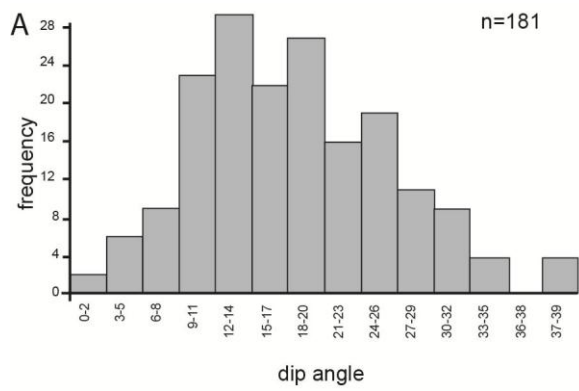


1000  
1001  
1002  
1003  
1004





1010  
1011



1012  
1013  
1014  
1015  
1016

